

**CONTROLLING THE PROPERTIES OF HOMOGENEOUS EPSILON
NEAR ZERO MATERIALS AND THEIR SWITCHING BEHAVIOR**

by

Mustafa Goksu Ozlu

A Thesis

Submitted to the Faculty of Purdue University

In Partial Fulfillment of the Requirements for the degree of

Master of Science in Electrical Engineering



School of Electrical and Computer Engineering

West Lafayette, Indiana

May 2022

THE PURDUE UNIVERSITY GRADUATE SCHOOL
STATEMENT OF COMMITTEE APPROVAL

Dr. Vladimir M. Shalaev, Chair

School of Electrical and Computer Engineering

Dr. Alexandra Boltasseva

School of Electrical and Computer Engineering

Dr. Alexander Kildishev

School of Electrical and Computer Engineering

Approved by:

Dr. Dimitrios Peroulis

*To my beloved sisters,
family and friends...*

ACKNOWLEDGEMENTS

First, I would like to pass my heartfelt gratitude to my Master's advisors Prof. Shalaev, Prof Boltasseva and Prof. Kildishev. It was an honor to be able to work with such leading scientists. They were not only great mentors but also inspring role models for what prominent researchers should be like. I would also like to thank all my group members for all their support and friendship with specifical thanks to my co-authors Dr. Colton Fruuhling and Dr. Soham Saha. Finally I am grateful to my family and my friends for their everlasting love, support and guidance.

TABLE OF CONTENTS

LIST OF TABLES	6
LIST OF FIGURES	7
ABSTRACT.....	9
1. INTRODUCTION.....	10
2. ALL OPTICAL SWITCHING AT ENZ.....	14
2.1 Introduction.....	14
2.2 Switching Mechanism of Homogeneous ENZ Materials	14
2.3 Semi Infinite Thickness and Optically Thick ENZ Films	18
2.4 Thin ENZ films.....	21
2.4.1 Thin ENZ film on glass	23
2.4.2 Thin ENZ film on metal	24
2.4.3 The ENZ mode	26
2.5 Effect of Drude Damping.....	27
2.6 Chapter Summary	29
3. THICKNESS DEPENDENT CONTROL OF AZO AND TiN OPTICAL PROPERTIES..	30
3.1 Introduction.....	30
3.2 Optical Properties and Crystalline Structure of TiN and AZO Films	31
3.2.1 Titanium nitride on silicon.....	31
3.2.2 Al-doped zinc oxide grown on titanium nitride films	37
3.3 Tailoring AZO-TiN Bilayers for Near Perfect Absorption.....	39
3.4 Dynamic Properties of TiN-AZO bilayers.....	42
3.5 Chapter Summary	44
4. SUMMARY.....	45
REFERENCES	46
VITA.....	68

LIST OF TABLES

Table 1 Optical properties of a hypothetical ENZ material described by Eq. (1).	18
Table 2 Optical properties of hypothetical metal.....	26
Table 3 The Drude-Lorentz Model Parameters of TiN Films on Si vs. TiN Thickness.....	32
Table 4 Figure of Merits of our grown polycrystalline TiN compared to other reported work on TiN	35
Table 5 The Drude-Lorentz Parameters of AZO Films on TiN vs. AZO thickness	37

LIST OF FIGURES

Figure 1 **a** A typical experimental setup for optical pump-probe experiments. An ultrafast laser pulse is generated and used to create a probe beam at the desired frequency. Schematics for interband and intraband pumping are shown on the sides. **b** The change in index of refraction for different relative changes in the plasma frequency $\Delta\omega_p/\omega_p$ near the ENZ point (denoted with vertical line). See Table 1 for the initial parameters of this plot. **c** A schematic of a dip in transmission as material is changed due to optical pumping. Two observation points are noted with vertical solid and dashed lines. The arrows indicate the direction of change seen by the observer. At the wavelength indicated by the solid line, increasing pump results in increasing the transmission. But under the same conditions, a probe at the dashed line observes first a decrease in transmission at low pump intensities, followed by an increase at higher intensities..... 16

Figure 2 **a** The unmodulated reflectance of TM polarized light from a semi-infinite ENZ material. Inset: reflectance of TE polarized light. **b** absolute change in reflectance for intraband pumping ($\Delta\omega_p/\omega_p = -0.12$). **c** The relative change in reflectance for the same conditions as **b**. The black vertical line is the unmodulated ENZ point. This is consistent for all similar figures. The red dashed lines are the Brewster θ_B and critical θ_c angles. 19

Figure 3 Modulated ($\Delta\omega_p/\omega_p = -0.12$) TM reflectance **a** and TM transmittance **b** from an ENZ material pumped with intraband laser. The inset of **a** shows the experimental configuration of the ENZ deposited on a glass substrate. The thickness of ENZ material is 900 nm. Fabry-Pérot modes can be seen in the lower left (small wavelength and small incident angle)..... 21

Figure 4 **a** Experimental configuration. A prism ($n_{prism} = 1.95$) is placed on top of a 10 nm ENZ film which is deposited on glass ($n_{glass} = 1.5$). **b** Unmodulated TM reflectance for the Kretschmann geometry. **c** Modulated absolute TM reflectance for interband pumping at 60-degree incident angle. The inset shows the modulation trend at the ENZ point as the modulation is increased. 23

Figure 5 **a** Configuration schematic. **b** Unmodulated TM reflectance as a function of wavelength and incident angle for 10 nm ENZ film on a metal substrate. **c** Modulated absolute TM reflectance for intraband pumping at 60-degree incident angle. The Drude parameters for the metal can be found in Table 2. The inset of **c** shows the trend of reflectance at the ENZ point. 25

Figure 6 **a** Experimental configuration. A prism ($n_{prism} = 1.95$) is placed on top of a 10 nm ENZ film which is deposited on glass ($n_{glass} = 1.5$). **b** Unmodulated TM reflectance for the Kretschmann geometry. **c** Modulated absolute TM reflectance for interband pumping at 60-degree incident angle. The inset shows the modulation trend at the ENZ point as the modulation is increased. 27

Figure 7 Transmission of a thin (40 nm) ENZ film deposited on glass. Same conditions as Fig. 4, except for the damping factor, which is **a** $\Gamma = 0.1\Gamma_0$, **b** $\Gamma = \Gamma_0$, and **c** $\Gamma = 2.5\Gamma_0$, where Γ_0 can be found in Table 1..... 28

Figure 8 (a) $\Re(\epsilon)$ of TiN on Si vs. thickness (b) $\Im(\epsilon)$ of TiN on Si vs. thickness (c) Plasmonic Figure of Merit vs. thickness (d) Plasma frequency (A_0) and Drude damping (B_0) vs. the film thickness..... 34

Figure 9 (a) Real part of permittivity of AZO on TiN vs thickness (b) Imaginary permittivity of AZO vs thickness (c) Plasma frequency (A_0) and Drude damping factor (B_0) vs thickness..... 38

Figure 10 (a) Reflectance spectrum of the ultra-subwavelength AZO on TiN for p-polarized light. (b) Ferrell-Berremann modes for p-polarized and (c) Fabry-Pérot modes for s-polarized light on the TiN-AZO films with varying TiN thickness. The solid lines in a-c are simulation results. The dashed lines are experimental results (d) Angle and Wavelength Dependent Absorption Spectrum of the AZO films obtained using the TMM method 42

Figure 11 (a) Schematic of the pump-probe setup (b) Color plot showing the reflectance modulation at a pump fluence of 1.5 mJ/cm^2 , at near infrared wavelengths (horizontal axis) versus time (vertical axis). (c) 90% of the signal decays under 10 ps, after which the relaxation is taken over by slower dynamics of the backreflectors. The plot shows the dynamics at a probe wavelength of 1350 nm. 43

ABSTRACT

One of the longstanding goals of photonics research has been to obtain strong optical nonlinearities. A promising method to achieve this goal is to operate in the so-called epsilon near zero (ENZ) spectral regime, where the real part of the dielectric permittivity changes sign. If accompanied by low losses, this region enables a platform to achieve extraordinarily high nonlinear response, along with many other interesting optical phenomena. In this work, some of the common all-optical switching structures employing homogeneous ENZ materials are investigated under varying conditions of frequency, incidence angle, and polarization. The optimum switching conditions have been highlighted to pave the way forward to the best experimental configurations in future studies. Moreover, the properties of some of the emerging novel plasmonic materials such as aluminum-doped zinc oxide (AZO) and titanium nitride (TiN) are investigated, specifically for ENZ applications. Their thickness-dependent crystalline structure and carrier densities are employed as a method to control their optical properties. A near-perfect absorption scheme is demonstrated utilizing the Ferrell-Berreman mode occurring at the ENZ region of ultrathin AZO and TiN film. The ENZ frequency and the associated absorption peak of AZO are engineered through thickness-dependence to cover most of the telecom range. This work covers the theoretical background for ENZ nonlinearities and looks into the materials aspect for better control of nonlinearities in experimental realizations.

1. INTRODUCTION

The propagation of light is governed by Maxwell's equations for which the electric field and the magnetic field components of the light are coupled. This mechanism gives rise to wave propagation where the time variation of the electric field and the magnetic field acts as sources driving each other. If the wave propagates inside a material, the charges inside the medium rearrange themselves and give rise to an additional polarization field. The contribution of magnetic and electric polarization fields can be thought of as introducing additional source terms to Maxwell's equations. In the end, the total response of the material can be expressed by the electric permittivity (ϵ) and magnetic permeability (μ) tensors which reduce to numbers for isotropic materials. For most materials, the magnetic response is weak and the magnetic permeability is equal to that of vacuum. Therefore, most of the information about a material's response to light can be inferred from the electric permittivity. Consequently, engineering or exploring materials with an exotic electric permittivity is a key step in controlling and modulating the light flow. For example, plasmonics employs the negative electric permittivity of metals to create better light confinement and strong field enhancement at the nanoscale^{1,2}. Similarly, high index dielectric materials are proposed for reducing the diffraction limit for low-loss light manipulation^{3,4}.

A new group of singular materials are the so-called epsilon-near-zero (ENZ) materials where the real part of the electric permittivity is close to zero. When the imaginary part, which is associated with losses, is low enough, the refractive index defined as the square root of permittivity also vanishes, giving rise to near zero index (NZI) behavior. In this case, the induced polarization field and the incident electric field cancel each other, killing the spatial variation throughout the medium. This causes the wavelength and the phase velocity of light to diverge to infinity. A plethora of applications utilizing these properties has been shown including light tunneling^{5,6}, photonic doping⁷, directional radiation⁸ and perfect absorption⁹⁻¹¹.

Apart from the aforementioned applications, ENZ materials most significantly enable exceptionally strong light-matter interactions. Although conventionally small, nonlinear effects are crucial in achieving all optical control of light, nonreciprocity and photonic circuitry. With

ENZ materials it is possible to achieve strong nonlinear effects with femtosecond recombination rate on the nanoscale.

The enhancement of the nonlinearities in the ENZ region is twofold. First, the group velocity in the ENZ region becomes diminishingly small as writing $v_g = d\omega / dk$ and expanding results in;

$$v_g = \frac{c\sqrt{\mu\varepsilon}}{\mu\varepsilon + \frac{\omega}{2}\left(\varepsilon\frac{d\mu}{d\omega} + \mu\frac{d\varepsilon}{d\omega}\right)} \quad (1.1)$$

which results in zero when the permittivity is zero. The near zero group velocity is known as the slow light effect^{12,13}, which increases the effective light-matter interaction time without the need for long interaction lengths. A second mechanism arises due to the enhancement of the field itself in the ENZ materials. Since the real part of the ENZ material's permittivity crosses zero, the normal component of the electric field is enhanced at the interface. This can be understood by examining the charge-free boundary conditions of the normal electric field component at the interface $\varepsilon_1 E_1^\perp = \varepsilon_2 E_2^\perp$, where the subscripts denote differing materials. These effects have been employed to demonstrate enhanced nonlinearities in the ENZ region including enhanced Kerr effect^{14,15}, all-optical switching¹⁶, frequency translation^{17,18} and enhanced third¹⁹⁻²¹ and high harmonic generation²².

One of the challenges of realizing the ENZ phenomena is finding the correct material platform with low enough losses that would give rise to NZI behavior. ENZ materials can be classified into two categories; homogeneous ENZ materials consisting of a single material employed at its crossing frequency and engineered structures showing artificial ENZ behavior. Engineered structures are employed when the naturally occurring materials are shorthanded. Also called heterogenous ENZ materials, these structures have the advantage of better tunability and lower losses, at the expense of higher complexity and larger size. Artificial ENZ metamaterials can be created employing waveguides at the cut-off frequency²³, hyperbolic metamaterials^{24,25}, and photonic crystal slabs at the Dirac Cone²⁶. Since the ENZ is an effective phenomenon, these structures need to be at least a couple wavelengths long.

Homogeneous ENZ structures have the advantage of having lower complexity and showing ENZ behavior locally. This is a crucial aspect as it enables ENZ materials to be integrated in other structures and have much smaller dimensions compared to structured heterogeneous ENZ materials. However, the lack of control of the ENZ wavelength and high material losses in many plasmonic material platforms is a major challenge for implementing homogenous ENZ materials.

Although many materials have natural crossing frequencies occurring in their dispersion diagram, the associated losses might be too high, and the position of the crossing might not coincide with the desired range. Common plasmonic materials like gold and silver have their crossing points in the ultraviolet region and have higher losses at their ENZ frequency. Novel plasmonic materials like transition metal nitrides, which proved to be a promising CMOS compatible platform with refractory properties^{27,28}, show better tunability, but high losses are still a challenge to overcome. Phononic materials (such as SiC) exhibit significantly lower losses but the crossing occurs in mid-IR range away from the telecom.

One promising homogeneous ENZ material class is transparent conducting oxides (TCOs). TCOs such as doped oxides of zinc or indium are advantageous because their ENZ regime is located in the telecom range (1.3 – 1.5 μm), and they exhibit low losses (small imaginary part of the electric permittivity)^{29,30} while offering an ultrafast response time on the scale of femtoseconds at the ENZ³¹⁻³³. Importantly, the optical properties of TCOs, including losses and the location of the ENZ region, can be effectively tailored by altering the growth/deposition conditions, thickness, and dopant ratio³⁴⁻³⁸. By utilizing TCOs as ENZ materials, ultra-fast switching^{31,39}, enhanced third harmonic generation^{19,40,41}, resonance pinning^{8,42-44}, optical time reversal⁴⁵, and adiabatic frequency conversion⁴⁶⁻⁴⁸ have been demonstrated.

In this work, first, we analytically investigated the optical switching behavior specifically for TCOs. Reflection and transmission modulation are outlined concerning a broad range of angles and wavelengths. The aim is to highlight an optimum structure for switching and to rigorously model the expected results for experiments. The second section consisted of an investigation of thickness dependent properties of homogeneous ENZ materials and its effect on ENZ related

absorption applications. Moreover, the characteristics of novel plasmonic materials are investigated in the respective chapter.

2. ALL OPTICAL SWITCHING AT ENZ

2.1 Introduction

The motivation of this chapter is to act as a primer, going through common experimental configurations and homogeneous ENZ schemes, particularly for all-optical switching experiments. We analyze the optical response of the structures in terms of their reflection and transmission when it is switched. The ENZ material used throughout this chapter is modeled as a TCO with comparable optical parameters as of those that have been reported in experimental studies. The findings of this part will help design the best configurations for pump-probe spectroscopy to extract how material properties change from the dynamic reflection and transmission data. These configurations also form the basis for more complex experiments such as time refraction⁴⁸, negative refraction in time-varying media⁴⁹, and photonic time crystal design⁵⁰. Understanding all-optical modulation through interband and intraband pumping serves as the first step to developing more complex experiments involving the dynamic modulation of epsilon-near-zero materials. Most of the data presented in this chapter are taken verbatim from the paper “Fruhling, C.; Ozlu, M. G.; Saha, S.; Boltasseva, A.; Shalaev, V. M. Understanding All-Optical Switching at the Epsilon-near-Zero Point: A Tutorial Review. *Applied Physics B: Lasers and Optics* **2022**, *128* (2), 1–12”.

2.2 Switching Mechanism of Homogeneous ENZ Materials

All-optical switching in ENZ materials is driven by modulating the refractive index, which in a non-magnetic material is given by $n = \sqrt{\epsilon}$. The change of the refractive index is then $\Delta n \propto \Delta\epsilon/\sqrt{\epsilon}$, which indicates that large changes in the index are expected near the ENZ point even for a small change in the permittivity⁵¹(Fig. 1b). This is one of the key advantages of using ENZ materials for all-optical switching^{31,52–54}. However, as seen in Fig 1b, the modulation of the refractive index is largest near the ENZ point but not exactly at it and the peak changes position with different levels of modulation. This is due to the nonzero imaginary permittivity and the shifting real permittivity with increasing pump fluence.

The permittivity can be modulated by optically pumping the material. We study the effects of optical pumping on ENZ materials using the Drude model^{55,56} that describes the permittivity of free electrons and can model reasonably well electrons in the conduction band. The permittivity is described as

$$\varepsilon = \varepsilon_{Re} + i\varepsilon_{Im} = \varepsilon_{\infty} - \frac{\omega_p^2}{\omega^2 + i\Gamma_0\omega} \quad (2.1)$$

$$\varepsilon_{Re} = \varepsilon_{\infty} - \frac{\omega_p^2}{\omega^2 + \Gamma_0^2} \quad (2.2)$$

$$\varepsilon_{Im} = \frac{\omega_p^2\Gamma_0}{\omega(\omega^2 + \Gamma_0^2)} \quad (2.3)$$

$$\omega_p^2 = \frac{Ne^2}{\varepsilon_0 m^*}. \quad (2.4)$$

In Eq. (1), ε_{∞} is the response in the high frequency limit, ω_p is the plasma frequency of the electrons in the conduction band and Γ_0 is the damping rate of plasma oscillations. The real and imaginary parts are given by Eqs. (2.2) and (2.3), respectively. In Eq. (2.4), for the plasma frequency, N is the electron number density, e is the charge, and ε_0 is the permittivity of free space. The effective mass m^* is defined as $m^* = \alpha m_0$, where α is a scalar quantity and m_0 is the mass of an electron in free space. If we assume a relatively small damping factor (which is valid for many TCOs at the ENZ point), the ENZ point occurs at $\omega_{ENZ} \approx \omega_p / \sqrt{\varepsilon_{\infty}}$. Therefore, one can use the plasma frequency to control the ENZ point and thus to control the amplitude and sign modulation of reflectance and transmittance. This also gives a means to control the spectral position of the resonance for thin ENZ films.

In TCOs, an optical pulse changes the plasma frequency (ω_p) by either changing the number density of free electrons (N) or the average effective mass (m^*). The bandgap energy supplies a natural distinction between two regimes of optical manipulation of the plasma frequency. For pump photon energies higher than the bandgap, electrons are promoted from valence to conduction band, which we call interband transitions (left Fig. 1a). Interband transitions naturally add more electrons to the conduction band and thus increase the plasma frequency^{32,57}. For photon energies less than the bandgap, intraband transitions move electrons to higher energies, (right Fig. 1a) where

due to the non-parabolic nature of the band structure the effective mass is increased^{58–60}. Thus, a decrease in the plasma frequency is expected^{32,53–55,61}. The changes to the optical properties happen on the sub-picosecond timescale. Eventually, the electrons either cool down (in case of intraband pumping) or recombine with holes in the valence band, and the material returns to its original state (in case of interband pumping) (Fig. 1a).

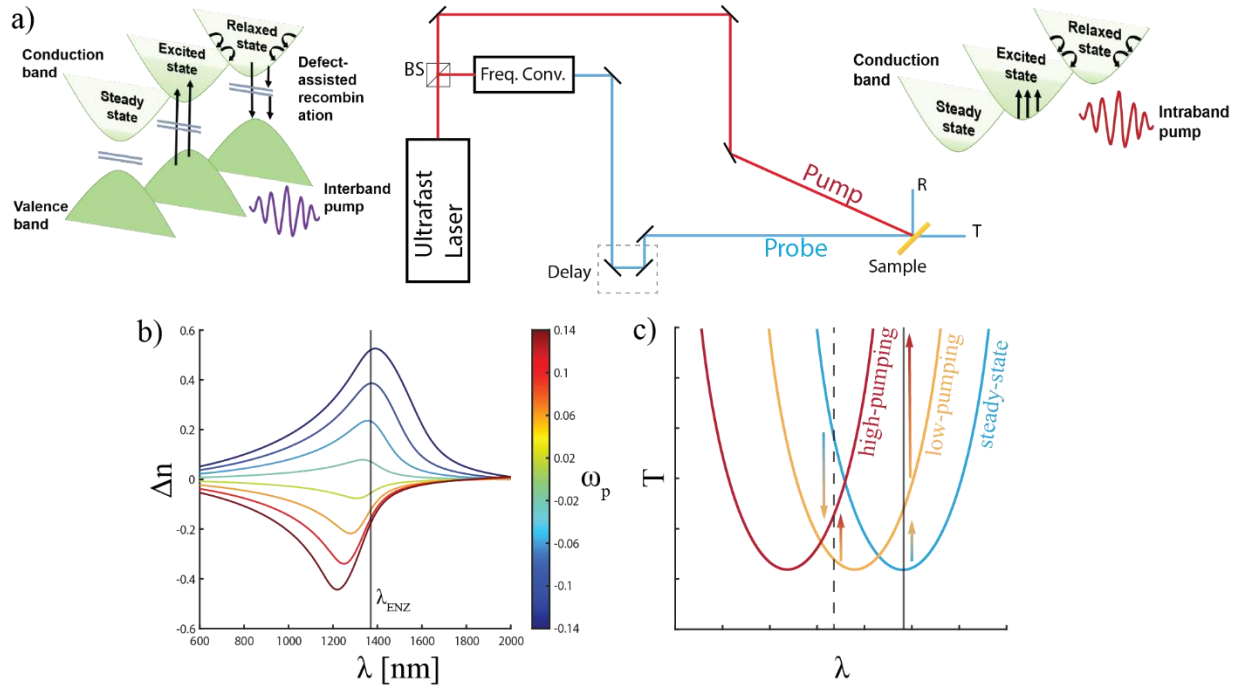


Figure 1 **a** A typical experimental setup for optical pump-probe experiments. An ultrafast laser pulse is generated and used to create a probe beam at the desired frequency. Schematics for interband and intraband pumping are shown on the sides. **b** The change in index of refraction for different relative changes in the plasma frequency $\Delta\omega_p/\omega_p$ near the ENZ point (denoted with vertical line). See Table 1 for the initial parameters of this plot. **c** A schematic of a dip in transmission as material is changed due to optical pumping. Two observation points are noted with vertical solid and dashed lines. The arrows indicate the direction of change seen by the observer. At the wavelength indicated by the solid line, increasing pump results in increasing the transmission. But under the same conditions, a probe at the dashed line observes first a decrease in transmission at low pump intensities, followed by an increase at higher intensities.

The damping factor in TCOs is also modulated by optical pumping. The rate of collisions between free electrons is described by the damping factor Γ_0 , and depends on the number density of electrons, which is increased by interband pumping. The damping affects the ENZ point, red-shifting it for larger values of Γ_0 and contributes to the width of optical resonances (see Sec. 5).

The center of Fig. 1a illustrates the conventional transient pump-probe experiment. In many experiments involving TCOs, the pump is a Ti-sapphire laser at the fundamental wavelength (~ 800 nm), or is frequency-converted by passing through a nonlinear crystal or an optical parametric amplifier. The probe pulse is a femtosecond pulse close to the ENZ wavelength of the material. The sources can vary depending on the type of the experiment, the kind of excitation targeted, and the ENZ point of the materials being investigated. The optical pump generates (interband) or excites (intraband) free carriers in the conduction band of a material, causing the electric permittivity and the refractive index to change. The probe pulse then measures changes in reflectance, transmittance, or both.

The measured response depends on the pump-pulse duration (10-100 fs), the probe-pulse duration (10-100 fs), and the material relaxation (typically ps-ns). The changed reflectance/transmittance measured at a specific pump-probe delay is generally an ‘average’ response during the probe’s temporal pulse-width which is short compared to the material relaxation. Under that assumption, our calculations of the dynamic changes measured by the probe pulse can be carried out with a static calculation. More complicated models have been employed that, for example, take into account the relaxation of the material using a two-temperature model^{54,62}

Intuitively, one might expect the change in the transmittance or the reflectance of a material at a particular wavelength to be monotonic. For example, an increasing interband pump generates free carriers, making the material more metallic, thereby decreasing the transmittance at longer wavelengths, and increasing the reflectance. However, we show that ENZ facilitated resonances – especially for thin films – complicate this intuitive picture. The reflectance and transmittance dynamics can exhibit nonmonotonic trends as the pump intensity is increased. As shown in Fig. 1c, the transmittance measured at one particular wavelength can be monotonically increasing, while at other wavelengths it can first decrease and then increase. This is experimentally relevant when measuring at the steady-state ENZ point, since the minimum of transmittance or reflectance may not occur at the exact ENZ point. We investigate the monotonicity of modulation for different pump-probe configurations in the subsequent sections of this tutorial.

The above analysis describes the physical framework for all-optical switching. However, we also need metrics to compare different configurations. An optical switch should be judged on its modulation depth between high and low states and the amount of pumping required to initiate switching. The switching is realized in the reflectance and transmittance changes which we scale to the incident power of the probe beam. Therefore, the switch with the best contrast will have an absolute change in reflectance or transmittance close to one and will have a relative change much greater than one. We now explore standard experimental configurations utilizing the concepts covered in this section. First, we discuss cases of optically thick layers of ENZ material and then move on to thin cases.

2.3 Semi Infinite Thickness and Optically Thick ENZ Films

The first experimental configuration to examine is the interface between a semi-infinite ENZ material and vacuum. The interaction between optical pump and ENZ is modeled using the Transfer Matrix Method (TMM)⁶³. TMM has been employed both for theoretical analysis⁶⁴ and for verifying experimental works⁶⁵. For all examples discussed below, unless stated otherwise, we use the initial parameters given in Table 1 for the ENZ material. Interband and intraband pumping are introduced by relative changes to the plasma frequency.

Table 1 Optical properties of a hypothetical ENZ material described by Eq. (1).

Drude Model parameters (unpumped)	Value
ϵ_∞	3
ω_p	2.4×10^{15} rads/s
f_p	3.8×10^{14} Hz
Γ_0	2.4×10^{13} Hz
λ_{ENZ}	1358 nm

The TMM models the reflectance, transmittance and absorptance. The steady-state reflectance of a semi-infinite ENZ material (Fig. 2a) generally increases with increasing wavelength across the ENZ point (vertical solid black line), as the material transitions from dielectric to metallic. Intraband pumping decreases the plasma frequency, thus raising the ENZ point and shifting the dielectric-metallic transition to higher wavelengths. The absolute modulation of the TM polarized reflectance $\Delta R_{TM} = R_{modulated} - R_{steady-state}$ (Fig. 2b) decreases to the right of the steady-state

ENZ point as the spectrum shifts. The modulation is greatest near the ENZ point where the dielectric-metallic transition occurs.

As with any semi-infinite case, common optical phenomena such as the Brewster angle and the critical angle for total reflection are apparent. The Brewster angle described by $\theta_B = \tan^{-1}(n_{ENZ}/n_{vac})$, curls from near the ENZ wavelength to approximately the 60-degree mark. This is the angle where tangential components of the TM polarized incident and transmitted wave exactly match at the boundary, and thus there is no reflected TM wave (impedance matching condition is met). The total reflection angle is described by $\theta_c = \sin^{-1}(n_{ENZ}/n_{vac})$, which for our example occurs between 25 and 90 degrees. Since the refractive index of the ENZ medium is complex due to absorption, the Brewster and the critical angle do not have their traditional meanings⁶⁶ derived for real refractive index, however, the effects can still be seen (Fig. 2)^{67,68}. For TM polarization, ENZ point shift induces the largest relative reflectance change $\Delta R_{TM}/R_{TM}$ along the Brewster angle where the steady-state reflectance is nearly zero (Fig. 2c). Because of the near zero reflectance at the Brewster angle, small changes in the absolute reflectance can be amplified into large relative changes, a technique utilized in extracting the carrier dynamics of materials through pump-probe spectroscopy. However, for all-optical switching, larger changes in the absolute reflectivity are desired.

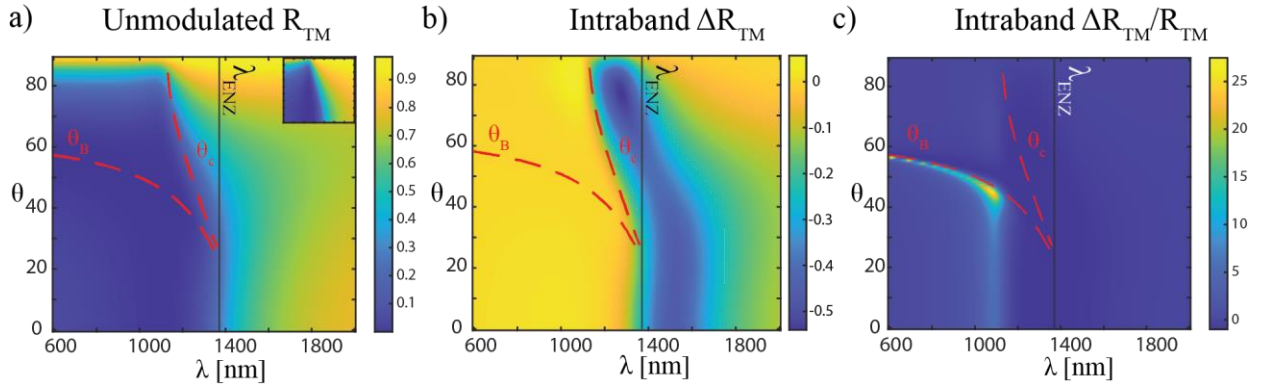


Figure 2 **a** The unmodulated reflectance of TM polarized light from a semi-infinite ENZ material. Inset: reflectance of TE polarized light. **b** absolute change in reflectance for intraband pumping ($\Delta\omega_p/\omega_p = -0.12$). **c** The relative change in reflectance for the same conditions as **b**. The black vertical line is the unmodulated ENZ point. This is consistent for all similar figures. The red dashed lines are the Brewster θ_B and critical θ_c angles.

These effects also are observed in the more practical case of optically thick ENZ layers (Fig. 3). Additionally, multiple reflections between surfaces results in the well-known Fabry-Pérot resonances for wavelengths smaller than the ENZ point. We consider a 900 nm ENZ film deposited on glass ($n_{glass} = 1.5$) and interfacing with vacuum on the other side. The 900 nm thickness was chosen so that Fabry-Pérot resonances are observed in Figure 3. The increasing interaction between surfaces also leads to a larger absorption at the ENZ point attributed to the electric field enhancement.

Clearly these configurations are capable of optical switching as we can see modulation on the order of $\Delta R_{TM} \sim 0.5$. The single step-like transition from non-reflecting to reflecting allows for a broadband optical switch that can be operated with both interband or intraband pumping. The relative change in reflection, however, is relatively small because of the large wavelength range over which the dielectric-metallic transition occurs leaving room for improvement. Even still, such optically thick configurations have been tested with great success.

For example, Kinsey et al.³¹ demonstrated picosecond amplitude modulation in optically thick aluminum-doped zinc oxide with an interband pump, while Clerici et al.³² showed even faster modulation is possible by combining both interband and intraband pumps. Modulation of the Fabry-Pérot modes has also been observed for example in Yttrium doped cadmium oxide (CdO) by Saha et al.³⁵. In telecommunication wavelengths where the optically thick CdO film is dielectric, moderate transmittance modulations of around 4% were observed. On the other hand, for the same film near the ENZ in the mid-infrared regime, a similar pump-fluence showed reflectance modulations of 135%, further underpinning the importance of ENZ induced modulation for lithography-free optical switching.

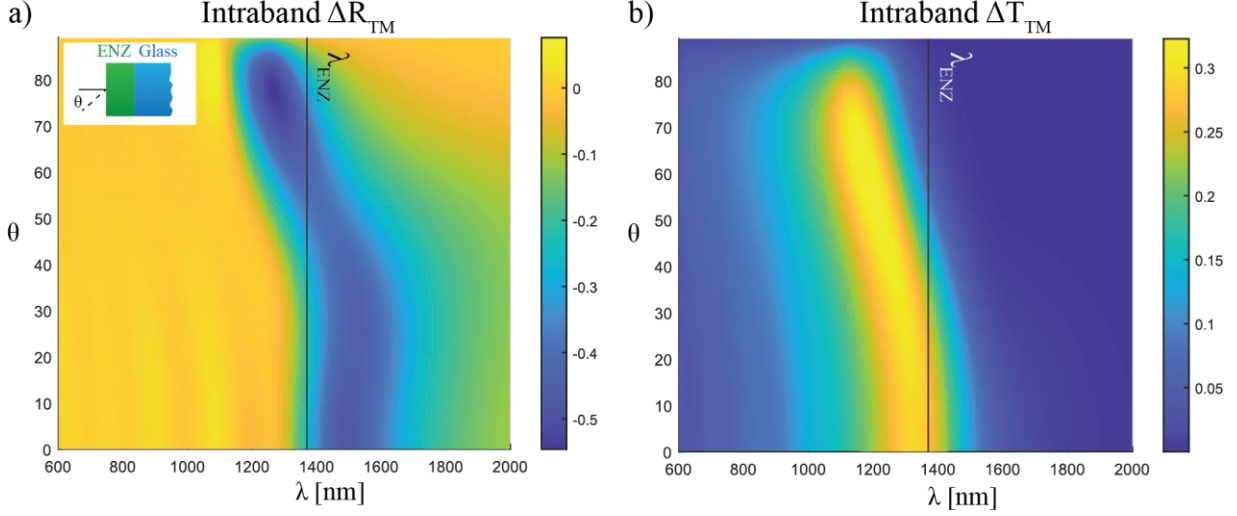


Figure 3 Modulated ($\Delta\omega_p/\omega_p = -0.12$) TM reflectance **a** and TM transmittance **b** from an ENZ material pumped with intraband laser. The inset of **a** shows the experimental configuration of the ENZ deposited on a glass substrate. The thickness of ENZ material is 900 nm. Fabry-Pérot modes can be seen in the lower left (small wavelength and small incident angle).

These configurations can also be used to study the optical properties of materials by performing pump-probe spectroscopy near their ENZ regime. The large changes in the relative reflectance minimum near the ENZ point makes such experiments quite useful for extracting otherwise hidden dynamics in materials. In such experiments, materials are pumped with a high-intensity laser pulse and a lower intensity probe pulse extracts the dynamics. This approach is particularly fruitful at the ENZ point where small changes in the index due to carrier dynamics are amplified.

For example, titanium nitride, a refractory ceramic used for many on-chip and hot-electron applications^{62,69}, has an ultrafast electron-phonon response time, which was not apparent in pump-probe spectroscopy experiments performed on it with a probe far from its ENZ value⁶². However, subsequent experiments on TiN and ZrN performed near their respective ENZ points showed this sub-picosecond relaxation time quite clearly, making a strong case for performing pump-probe experiments for material characterization near the materials' ENZ points⁵².

2.4 Thin ENZ films

As the thickness of the ENZ layer decreases beyond the skin depth, the non-radiative surface modes on the upper and lower boundaries start to couple and split into symmetric (long-range) and

antisymmetric (short-range) modes⁷⁰. If the film thickness is further reduced, these two modes become even more distinctive, and the symmetric mode forms a flat dispersion curve at the ENZ spectral region called the ENZ mode. The flat dispersion of the ENZ mode implies a reduction of the group velocity that is often referred to in slow light schemes⁷¹⁻⁷³. Additionally, there is a mode in the radiative region around the ENZ point known as the Ferrell-Berreman (FB) mode⁷⁴⁻⁷⁶. When light couples into any of these modes, a large absorptance (reflectance/transmittance) peak (dip) is observed. Optical pumping is then used to shift the peak (dip) resulting in giant reflectance or transmittance modulations due to the narrow resonant features (Fig 1.c). We separate the resonances as the radiative and bound (non-radiative) modes.

The radiative FB modes occur in subwavelength films at slightly lower wavelengths than the ENZ point and to the left of the light line. This allows the advantageous coupling of light from free space without the need of a special geometry or pattern^{53,77}. Coupling generally requires the incident wavevector to have a nonzero transverse component and is achieved in configurations where a subwavelength ENZ film lies on top of another medium acting as a back-reflector. The phenomenon is named after R. A. Ferrell⁷⁴ who showed an absorption peak near the plasma frequency for thin plasmonic films and D. W. Berreman⁷⁵ who showed a similar absorption for phononic thin films near the longitudinal phononic resonance that occurs in the optical frequency range.

The bound ENZ mode occurs on the right side of the light line and is therefore not accessible via direct optical excitation. A common configuration to excite ENZ modes is to use the Kretschmann geometry⁷⁸⁻⁸¹ where a prism is placed on an ENZ film. The refractive index and incident angle into the prism are used to match the projection of the light momentum along the interface to the ENZ dispersion. This meets the phase-matching condition and excites the ENZ mode. Gratings are also used in a similar capacity to meet the phase-matching conditions⁷⁷. In the literature, the static characteristics of the FB and ENZ modes have been studied in detail^{64,80,82,83}. Here, we focus on the modulation around those modes with optical pumping.

2.4.1 Thin ENZ film on glass

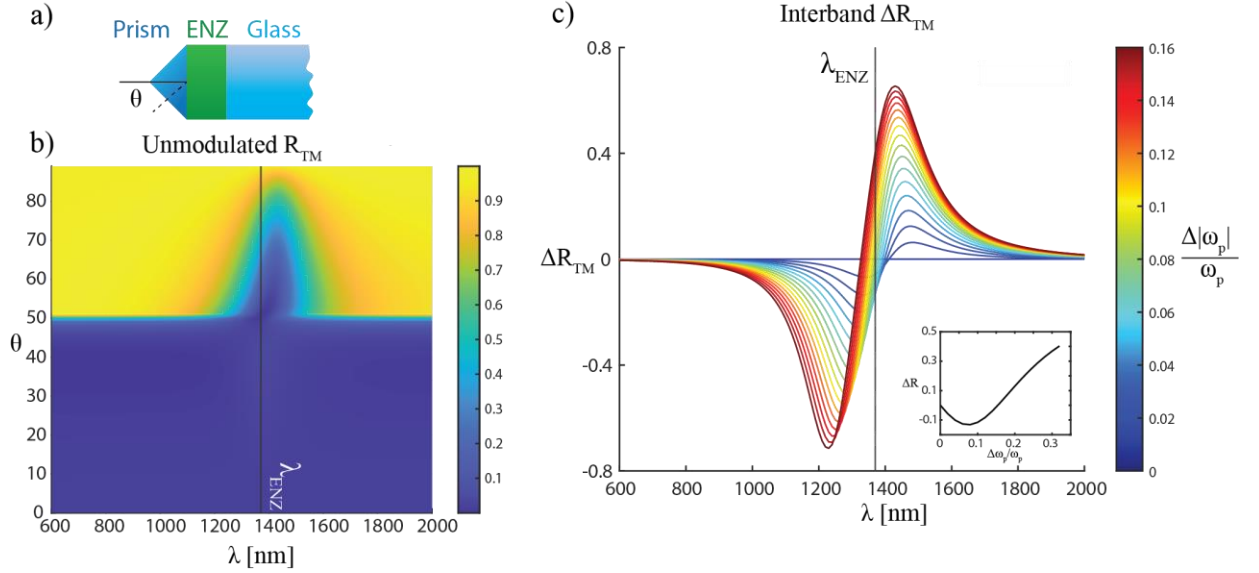


Figure 4 **a** Experimental configuration. A prism ($n_{prism} = 1.95$) is placed on top of a 10 nm ENZ film which is deposited on glass ($n_{glass} = 1.5$). **b** Unmodulated TM reflectance for the Kretschmann geometry. **c** Modulated absolute TM reflectance for interband pumping at 60-degree incident angle. The inset shows the modulation trend at the ENZ point as the modulation is increased.

First, we consider a 40 nm ENZ film deposited on glass (Fig. 4a, inset). In this configuration, the film supports a radiative mode that can be excited directly by light from free space. The steady-state absorption in Fig. 4a has a peak slightly to the left of the ENZ point. The large absorption leads to a local minimum in the transmittance at the ENZ point similar to the schematic in Fig. 1c. Therefore, non-monotonic behavior is expected when measuring the transmittance at the ENZ point. A monotonically increasing pump-fluence can result in a sign reversal of the transmittance modulation.

An interesting example is found by inspecting at the 60-degree angle of incidence shown in Fig. 4b-d. Some wavelengths have monotonic behavior when the colors from blue to red do not overlap. For example, at the ENZ wavelength for both transmittance plots (Fig. 4c, d), the modulation increases monotonically with increasing pump fluence. At other wavelengths the colors overlap showing a non-monotonic behavior. Examples of this are seen at the ENZ wavelength for reflectance and the dashed lines in the transmittance plots (see insets). The sign reversal of the

optical response can have an important impact when trying to retrieve optical properties from experimental data. Especially for nonlinear processes, it is common to measure reflectance/transmittance and then recover the nonlinear susceptibility from those measurements^{84,85}. A sign reversal might then be erroneously attributed to an incorrect sign of the susceptibility.

We appraise this configuration for its prospects in optical switching by evaluating the modulation depth and maximum relative modulation. The steady-state reflectance is small for all angles because the thin ENZ film does not reflect much light and glass is also transparent. Therefore, reflectance is a poor choice for optical switching because the depth of modulation is small. This is evident when investigating the steady-state reflectance at the ENZ point, where $R_{TM} \sim 0.1$ and the maximum modulation is $\Delta R_{TM} \sim 0.01$ (Fig. 4b inset). The transmittance cases show a larger change of nearly $\Delta T_{TM} \sim 0.5$ at selected wavelengths. However, the unmodulated transmittance at 60 degrees is $T_{TM} \sim 0.5$, making the relative change small. Transmittance is the better of the two but does not meet both the criteria of large relative change ($\Delta T_{TM}/T_{TM} \gg 1$) and a large depth of modulation ($\Delta T_{TM} \sim 1$).

2.4.2 Thin ENZ film on metal

Another common experimental configuration is a thin layer of ENZ material deposited on a metal substrate^{33,80,86-88}(Fig. 5a). The Drude model is used here to describe the metal substrate with the parameters shown in Table 2. This is another example of a radiative mode where a large absorption peak exists near the ENZ point. The transmittance in this case is negligible and the reflectance is high because of the metal layer. The reflectance shows a dip where the absorption is the highest (Fig. 5b) that can be used for optical switching. The reflectance dip follows parallel to ENZ wavelength for lower incident angles and diverges to the ENZ-metal surface polariton resonance at higher angles. The offset of the minimum from the ENZ wavelength causes a probe at the ENZ wavelength to experience nonmonotonic reflectance for intraband pumping (Fig. 5c inset).

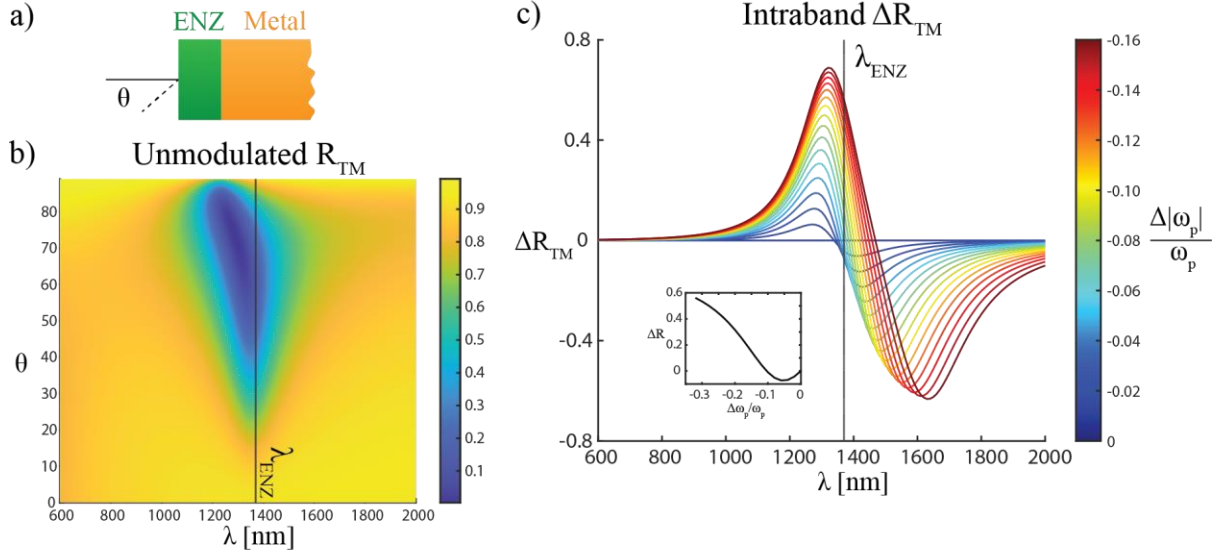


Figure 5 **a** Configuration schematic. **b** Unmodulated TM reflectance as a function of wavelength and incident angle for 10 nm ENZ film on a metal substrate. **c** Modulated absolute TM reflectance for intraband pumping at 60-degree incident angle. The Drude parameters for the metal can be found in Table 2. The inset of **c** shows the trend of reflectance at the ENZ point.

The large contrast of the reflectance dip motivates the use of this configuration for all-optical switching and both interband and intraband pumping are applicable. For larger angles of incidence ($\theta > 60$), the reflectance dip is not symmetric around the minimum, therefore interband and intraband pumping require different intensities to achieve the same switching contrast. Intraband pumping is then slightly favorable because the transition from low to high reflectance happens over a shorter wavelength range requiring less modulation of the plasma frequency.

Comparing the absolute reflectance change in Fig. 5c. to the changes in Fig. 4, we see a larger absolute modulation for improved switching. At some wavelengths $|\Delta R_{TM}| > 0.6$, such as at $\lambda = 1320$ nm where the relative reflectance change is approximately 10-times. Both the relative change and the modulation depth are large here making this configuration a better candidate for switching (recall that reflectance and transmittance are scaled to one). This also illustrates how the ENZ wavelength is not always the best suited for all-optical switching since the largest modulation for 60-degree angle of incidence is at $\lambda = 1320$ nm and the ENZ wavelength is $\lambda_{ENZ} = 1380$ nm. The FB mode illustrated in this example has been used for femtosecond polarization switching by Yang et al³³. A linearly polarized probe beam with both TE and TM components was incident on

doped CdO deposited on gold and a pump beam was used to modulate the ENZ point. The reflectance was modulated from $R_{TM} = 0.01$ to $R_{TM} = 0.86$ in the TM component, while the TE component had no observable modulation. Taking advantage of the different absorptance for TE and TM polarized light near the ENZ point, an optically controlled polarization switch was demonstrated by either increasing or decreasing attenuation of the reflected TM light.

Table 2 Optical properties of hypothetical metal

Drude Model parameters	Value
ϵ_{metal}	3.5
$\omega_{p_{metal}}$	$9.6 \times 10^{15} \text{ rad/s}$
Γ_{metal}	$4.8 \times 10^{13} \text{ s}^{-1}$

2.4.3 The ENZ mode

Exciting the ENZ mode requires a special geometry such as the Kretschmann geometry using a prism. For our calculations, we assume that a prism with a refractive index of 1.95 is placed on a 10 nm ENZ film on a glass substrate ($n_{glass} = 1.5$). A schematic of the configuration is shown in Fig. 6a, where angle of incidence is defined with respect to the normal of ENZ film and not the prism, to make comparing with previous examples easier. The ENZ layer needs to be deeply subwavelength to observe the ENZ mode⁶⁴ and because of that a clear line at approximately 50 degrees shows the total reflection angle corresponding to the prism-glass critical angle. At angles larger than 50 degrees, the ENZ mode is visible as a dip in the reflectance spectrum (Fig. 6b). Investigating again along the 60-degree angle of incidence (to compare with previous cases), we see a similar amount of modulation in the reflectance as in the FB mode. In contrast, the dip in this case is at larger wavelengths than the ENZ point, where for the FB mode it is at smaller wavelengths. Therefore, the ENZ mode is equally viable as an optical switch compared to the FB mode.

A similar configuration was utilized by Bohn et al., where a 60 nm ITO film was placed on a prism and exposed to air. Using the coupling between pump and probe beam they reported reflectance changing from $R_{TM} = 0.01$ to $R_{TM} = 0.45$ with ultrafast switching speeds⁵³. By probing away

from the reflectance minimum, they also observed the ultrafast non-monotonic behavior of reflectance as the pump pulse shifted the reflectance minimum through the probe wavelength. This exact behavior is seen in the inset of Fig 6c., where a sweeping of modulation intensity shows first a decrease, and then increase in reflectance. This brings about an important point that the ENZ modulation may not be monotonic during the interaction with a pulsed laser as intensity ramps up. This is especially important for cases where the probe-pulse duration is less than the pump-pulse duration, which is often true for pump-probe experiments.

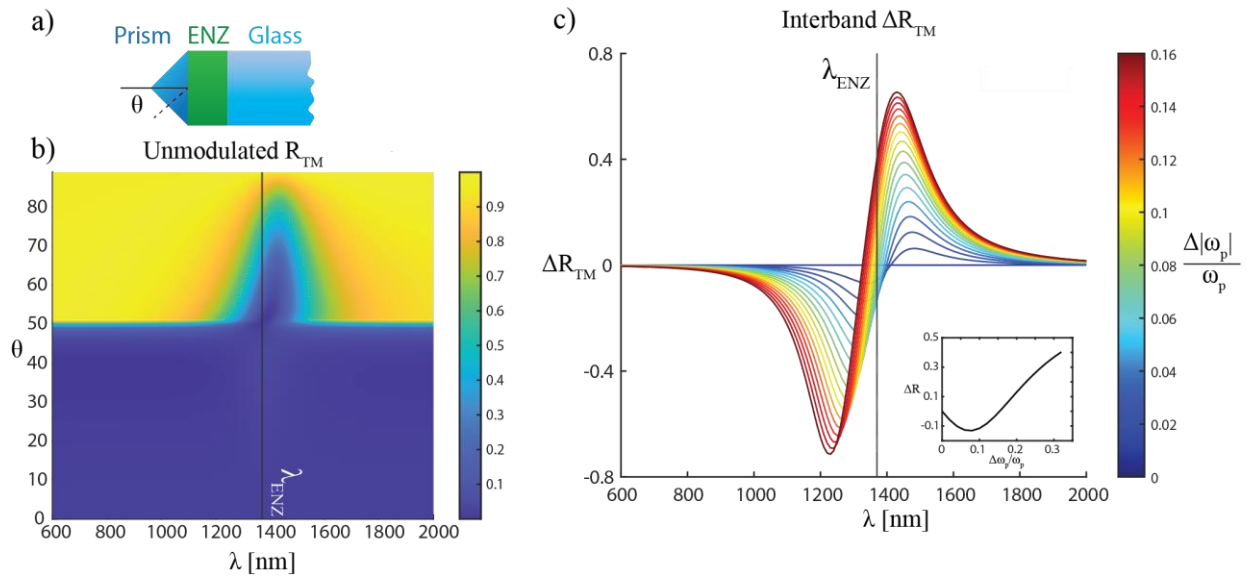


Figure 6 **a** Experimental configuration. A prism ($n_{prism} = 1.95$) is placed on top of a 10 nm ENZ film which is deposited on glass ($n_{glass} = 1.5$). **b** Unmodulated TM reflectance for the Kretschmann geometry. **c** Modulated absolute TM reflectance for interband pumping at 60-degree incident angle. The inset shows the modulation trend at the ENZ point as the modulation is increased.

2.5 Effect of Drude Damping

In the previous examples, we assumed that photoexcitation of free-carriers only changed the plasma frequency by increasing the free-carrier concentration or their effective mass. However, damping also plays an important role in all-optical switching. The damping factor represents the inverse of the scattering time for free electrons and is therefore related to the electron density⁸⁹. Optical pumping has been shown to change the damping factor^{33,55,60,90,91} and depending on experimental factors it can either decrease or increase.

The resulting change in damping factor due to optical pumping modulates the ENZ point. Re-examining the ENZ frequency derived from Eq. (2) while including the effect of damping results with $\omega_{ENZ} = \sqrt{\omega_p^2/\epsilon_\infty - \Gamma_0^2}$. We can estimate the size of this effect by comparing terms under the square root sign. For typical experimental values $\Gamma_0/\omega_p \leq 1/10$ and the correction is small. There is a stronger effect from damping changes on the ENZ resonance width.

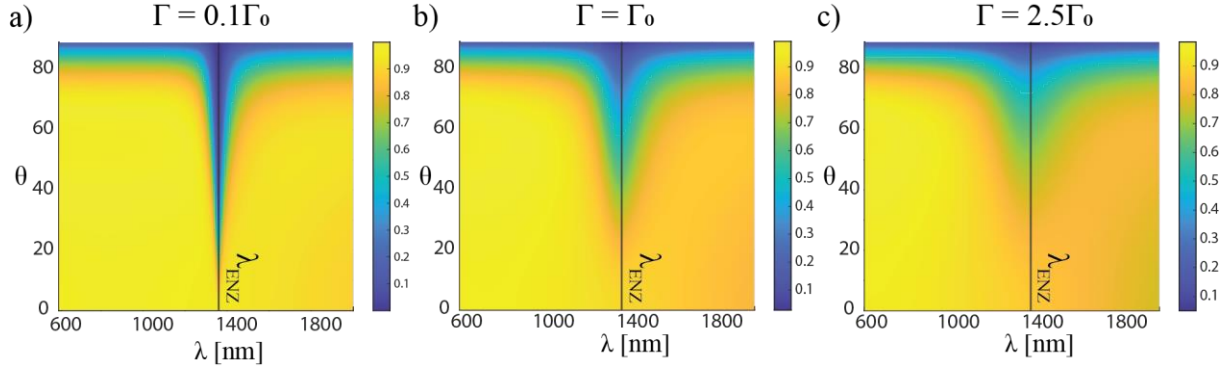


Figure 7 Transmission of a thin (40 nm) ENZ film deposited on glass. Same conditions as Fig. 4, except for the damping factor, which is **a** $\Gamma = 0.1\Gamma_0$, **b** $\Gamma = \Gamma_0$, and **c** $\Gamma = 2.5\Gamma_0$, where Γ_0 can be found in Table 1.

An illustrative example is made by examining the spectral width change for a thin ENZ layer like that in Fig. 4. We considered three cases of differing damping constants shown in Fig. 7, where all other parameters are the same as in the thin ENZ case. We plot the steady-state transmission of TM polarized light through the thin film showing drastic changes in the resonance width with varying damping factors; careful inspection also reveals a shift in the absorption peak indicating a change in the ENZ point.

The immediate conclusion from this example with regards to ultrafast optical switching is the need to keep the damping constant small for a narrow resonance. A narrow resonance allows for sharper changes in the transmittance and reflectance, at lower pumping intensities. For example, if we consider the 60-degree incidence angle, the half width of the transmission dip is ~ 80 nm for the case of Fig. 7a. The unmodulated transmittance is $T_{TM} \sim 0.04$. Using a plasma frequency modulation of $\Delta\omega_p/\omega_p = 0.15$, the transmittance increases by 20 times. In contrast, for the same plasma frequency modulation, the change in the case of Fig. 7b is at most a factor of two and less than one tenth change for Fig. 7c. The losses should then be tailored to accommodate the switching

specifications. Low losses should be used for efficient narrow-band switches while moderate losses may be more applicable for broadband switching.

2.6 Chapter Summary

In this chapter we study the modulation of the reflectance and transmittance of various ENZ media, with interband and intraband optical pumping by using the Drude model. We discuss the effects of pumping on the plasma frequency and employed the TMM to analyze experimental configurations. The cases studied here point out general aspects for all-optical switching with ENZ materials. Firstly, the use of ENZ materials greatly increases the modulation of the refractive index. Secondly, thin films demonstrate absorption peaks near the ENZ wavelength because of the strong interaction between surface waves. The absorption peaks imply a dip in transmittance or reflectance that can be shifted with optical pumping. This causes substantial changes in the reflectance or transmittance allowing such systems to be utilized for all-optical switching. Finally, losses due to damping affect the ENZ point and the resonance width. There is a tradeoff where larger damping factors broaden the resonance allowing for broadband switching. However, the depth of the absorption is reduced and makes the contrast between switching states smaller. Oppositely, lower damping factors have a narrower resonance that reduces the optical switch bandwidth, but increases the switch contrast.

We also show that although the largest modulations occur proximal to the ENZ point, the ENZ point itself is not always the best wavelength for optical switching. For example, the Ferrell-Berremann mode or ENZ mode are excited above and below the ENZ wavelength respectively, resulting in the maximum modulation occurring away from ENZ point. Deviations of the wavelength away from the maximum/minimum results in a non-monotonic trend of the reflectance or transmittance as a function of the optical pumping power. Therefore, it is critical to optically characterize ENZ materials in the steady state, so that the unpumped ENZ point and nearby resonances are well identified. The pump power along with the pump photon energy are also important parameters in experiments. These effects should be carefully considered, especially when tracking the changes in reflectance or transmittance to extract the optical properties in the photoexcited state.

Throughout, we have discussed multiple common experimental configurations and ENZ schemes, focusing on all-optical switching. These configurations are building blocks for understanding and constructing more complex experiments such as those involving time refraction⁴⁸, time reflection⁵⁰, negative refraction⁴⁹ and four-wave mixing⁹², where the ultrafast refractive index transitions from optical switches may be used.

3. THICKNESS DEPENDENT CONTROL OF AZO AND TIN OPTICAL PROPERTIES

3.1 Introduction

The aim of this chapter is to explore the thickness dependent optical properties of novel plasmonic materials and its effect on their ENZ properties. Titanium Nitride (TiN) and Aluminum doped zinc oxide (AZO), respectively belonging to Transition Metal Nitrides and Transparent Conducting Oxides, are investigated and a bilayer structure exhibiting Ferrel-Berremann modes are investigated statically and dynamically. The ENZ point and the associated applications are tuned across the telecom wavelengths.

Titanium nitride is a promising material for nanophotonic applications because of its good plasmonic properties⁹³, CMOS compatibility⁹⁴, tailorability^{95,96}, versatility of fabrication techniques⁹⁷⁻⁹⁹, and high laser- and thermal tolerance¹⁰⁰⁻¹⁰². These attractive features have led to its utilization in high-temperature photovoltaics¹⁰³, optical circuitry^{104,105}, nonlinear optical devices^{100,106}, and many other practical applications. Similarly, transparent conducting oxides (TCOs) form another class of optical materials for dynamically controlled nanophotonics spanning optical switching¹⁰⁷, electroabsorption modulators^{108,109}, tunable metasurfaces^{110,111}, and nonlinear experiments employing epsilon-near-zero (ENZ) physics^{15,19,112-114} for novel applications that now include ultrafast switching^{16,115,116}, tunable broadband light absorption^{11,117-119}, enhanced second-harmonic¹²⁰ and high harmonic¹²¹ generation.

For these technologically relevant materials, the optical properties can be controlled during growth by varying deposition conditions. For example, the properties of titanium nitride can be tailored by fine-tuning the temperature, gas ratio, and even post-deposition annealing^{97,122,123}. The optical

properties and the ENZ resonances of conducting oxides can also be altered by varying the growth conditions, namely the gas ratio, the dopant concentrations, or post-deposition annealing^{97,109,124,125}. However, a simpler method of tailoring such conducting oxides and nitrides is often overlooked. The conductivity of materials, an intrinsic material property, is strongly affected by the film thickness due to changes in the carrier concentration, crystalline properties, and surface roughness^{126–129}, especially for thin films. It stands to reason that film thickness should also play a role in the optical property of conducting materials, and in turn, be used to control device characteristics. This work explores the thickness-dependence of the optical properties of polycrystalline titanium nitride (TiN) and aluminum-doped zinc oxide (AZO) and how these materials can be tailored for select passive and dynamic photonic applications, especially those utilizing the ENZ properties of the constituent thin films. Most of the data in this chapter is taken verbatim from the paper; “S. Saha, M. G. Ozlu, S. N. Chowdhury, B. T. Diroll, R. D. Schaller, A. Kildishev, A. Boltasseva, and V. M. Shalae, "Tailoring the Thickness-Dependent Optical Properties of Conducting Nitrides and Oxides for Epsilon-Near-Zero-Enhanced Photonic Applications," (2022).”

3.2 Optical Properties and Crystalline Structure of TiN and AZO Films

3.2.1 Titanium nitride on silicon

Titanium nitride in its epitaxial form has been utilized in absorbers,¹⁰¹ waveguiding,^{104,105} refractory plasmonics,^{100–102} plasmonic nanoparticle lattices,¹³⁰ and physics with ultrathin films.¹³¹ However, epitaxial film growth requires lattice-matched substrates, which limits their application in an industry-compatible setting.²⁸ This difficulty makes it essential to grow and characterize optical-quality films of polycrystalline titanium nitride on non-lattice-matched substrates.

To investigate the effect of thickness on the optical response of polycrystalline TiN films, we grew TiN films of several thicknesses on silicon by DC reactive magnetron sputtering at elevated temperatures. This method was utilized to produce optical grade TiN by other groups^{132–134}. Alternative techniques of growing TiN include pulsed laser deposition^{130,135} and atomic layer deposition¹³².

A 99.995% pure Ti target of 2-inch diameter was used for the process. To ensure uniformity, the distance from the target to the source is kept at 20 cm. The chamber is pumped down to 10^{-8} Torr to prevent oxygen contamination, and is backfilled with Ar to a pressure of 5 mTorr. The Ti is sputtered for 2 minutes to clean the top surface with a power of 200W, and then an Ar:N₂ mixture of 1:18 is used for the sputtering process. The substrate is heated to a temperature of 800°C and rotated at 5 rpm. We note that it is possible to grow epitaxial titanium nitride on silicon, but complicated cleaning procedures are required to remove the native oxide layer¹³⁶. For this study, we wanted to focus on the evolution of the optical properties of polycrystalline titanium nitride with thickness. The TEM image of the films is given in Figure 8 showing the polycrystalline structure.

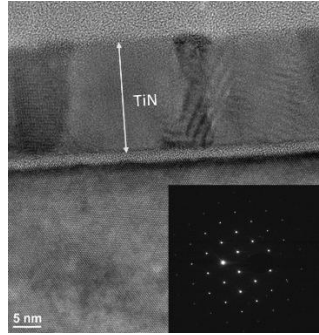


Figure 8 TEM image of the 60 nm TiN film, showing the polycrystallinity. The inset shows the diffraction pattern of the film.

We measured the optical properties of the TiN films with spectroscopic ellipsometry, and fitted them with a Drude-Lorentz model¹³⁷, with one free electron term and two Lorentz oscillator terms with the resonance positions at higher energy levels. The parameters of the full model are given in table 3 for the films grown with different thicknesses.

Table 3 The Drude-Lorentz Model Parameters of TiN Films on Si vs. TiN Thickness

Thickness	10 nm	25 nm	60 nm	130 nm	200 nm
A ₀	46.782	51.595	49.550	41.055	40.152
B ₀	0.378	0.258	0.217	0.193	0.227
A ₁	98.232	98.232	52.954	31.801	28.517
B ₁	2.157	2.157	1.364	0.661	1.003
E ₁	5.119	5.119	4.466	4.117	4.117
A ₂	407.280	407.280	310.930	357.600	391.660

B ₂	149.950	149.950	79.364	80.546	99.451
E ₂	5.982	5.982	4.044	3.945	4.748
ε _∞	2.26	2.84	3.39	3.20	3.41
MSE	5.8	2.8	4.1	8.9	8.7

In the telecommunication range, the contribution of free-electrons, represented by the Drude term, strongly governs the optical response. Then, the real and the imaginary parts of the permittivity can be written separately as,

$$\varepsilon_1 = \varepsilon_b - \frac{A_0}{(\hbar\omega)^2 + B_0^2} \quad (3.1)$$

$$\varepsilon_2 = \frac{A_0 B_0}{\hbar\omega((\hbar\omega)^2 + B_0^2)} \quad (3.2)$$

where ε_b denotes the net contribution of the Lorentz oscillators with background permittivity ε_∞. The dielectric function of TiN films with different thicknesses are plotted in Figure 9.

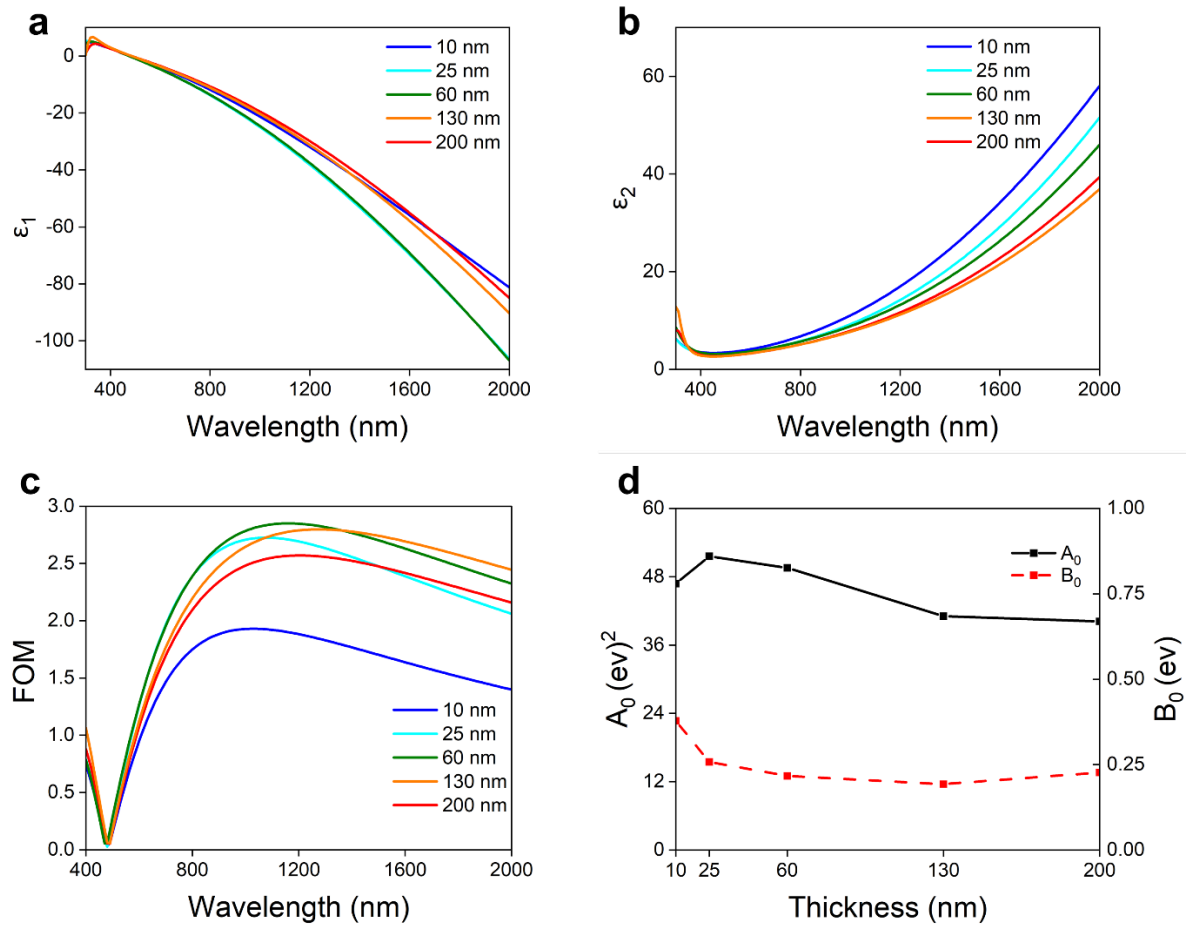


Figure 9 (a) $\Re(\epsilon)$ of TiN on Si vs. thickness (b) $\Im(\epsilon)$ of TiN on Si vs. thickness (c) Plasmonic Figure of Merit vs. thickness (d) Plasma frequency (A_0) and Drude damping (B_0) vs. the film thickness

At first, as the thickness increases up to 25 nm, the slope of the real part of the TiN dielectric function becomes steeper, implying increased metallicity (see Fig. 9a). The figure indicates that when the thickness is approaching 60 nm, the change of the real part is saturating. For the imaginary part of the TiN dielectric function (ϵ_2) this dependence is different; as the film thickness decreases from 130 nm to 10 nm, we observe an increase that indicates increasing absorptive losses (Fig. 1b). Figure 1c plots the so-called plasmonic figure of merit (FOM) of the films, defined as the absolute value of the ratio of the real part of the permittivity to the imaginary part.^{138,139} The grown TiN films have figure of merits better than the majority of the reported polycrystalline films, and comparable to that of some epitaxial films^{28,93,140–144}. Table 4 shows the comparison of the FOM between the TiN films grown in this work and the TiN films that has grown in previous

works. The table highlights the distinguished quality of the films in comparison to other polycrystalline films.

Table 4 Figure of Merits of our grown polycrystalline TiN compared to other reported work on TiN

Reference	Growth Technique	Morphology	FOM at 700nm	FOM at 1550nm
Guru 2012 ²⁸	Magnetron Sputtering	Polycrystalline	0.2	0.8
Guru 2012 ²⁸	Magnetron Sputtering	Epitaxial	1	1
Dal Negro 2015 ¹⁴⁵	Magnetron Sputtering	Polycrystalline	1	1
Huber 2001 ¹⁴⁶	ME-PIII	Polycrystalline	1.2	
Patsalas 2001 ¹⁴⁷	Magnetron Sputtering	Polycrystalline	1.25	-
Evelyn Hu 2015 ¹⁴⁰	Magnetron Sputtering	Epitaxial	1.42	2.7
Nagao 2018 ¹⁴⁸	PLD	Polycrystalline	1.5	1.3
This Work	Magnetron Sputtering	Polycrystalline	1.7	2.72
Hu 2019 ¹³³	Magnetron Sputtering	Polycrystalline	1.75	1.9
Langereis ¹⁴⁹	ALD	Epitaxial	1.9	2.2
Kinsey 2020 ¹⁴¹	ALD	Epitaxial	2	2.33
Kinsey 2021 ¹⁵⁰	ALD	Epitaxial	2	2.4
Odom 2017 ¹⁴²	Magnetron Sputtering	Epitaxial	2.3	-
Gall 2001 ¹⁵¹	UHV Sputtering	Epitaxial	2.3	-
Maurya ¹⁵²	molecular beam epitaxy	Epitaxial	2.8	3.23
Hu 2019 ¹³³	Magnetron Sputtering	Epitaxial	3	3.7

To understand the change in the optical response with the thickness, we investigate the crystalline structure of the TiN and its permittivity model. The plasma frequency increases for thicknesses up to 25 nm then starts decreasing (Fig. 9d). An increase in the plasma frequency causes both the real and the imaginary part of the permittivity to increase.

The plasma frequency is related to carrier concentration and the effective mass of the electrons through the equation $\hbar^{-1}\sqrt{A_0} = \omega_p = e\sqrt{\frac{N}{m^*\epsilon_0}}$. The plasma frequency of polycrystalline films is lower (A_0 between 43-51.6 (eV)²) than that of epitaxial titanium nitride films ($A_0\sim 58$ (eV)²) reported in previous studies^{105,153}. This is because of the columnar growth of the polycrystalline films seen from TEM (Figure 8), with many grain boundaries, through which oxygen diffuses into the lattice, lowering the carrier density¹⁵⁴⁻¹⁵⁶.

The 10-nm-thick films have the highest damping factors attributed to the increased collisions of electrons with the surface. A similar effect was observed by Shah et al. in a previous study, where the damping factor of TiN thin films increased with decreasing thickness¹⁵⁷. AFM images (Figure 10) show that the thicker films have more well-defined and bigger grains. For thicker films, the damping factor generally decreases due to increased grain size, leading to a decreased collision of carriers with the grain boundaries. The films have a surface roughness of less than ~ 3.5 nm, which is higher than in atomically-flat epitaxial films, yet comparable to polycrystalline films reported previously^{130,135}. Overall, the dielectric function of the studied TiN films shows a strong dependence on the thickness, adding a critical degree of control over their optical response

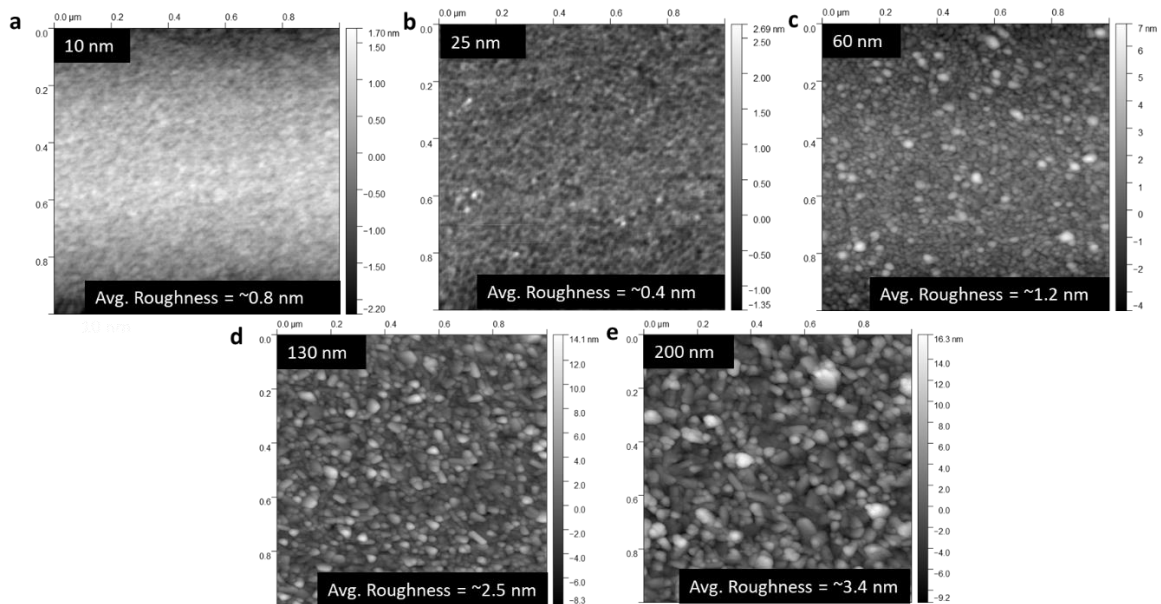


Figure 10 AFM image of TiN films with different thicknesses of (a) 10 nm, (b) 25 nm, (c) 60 nm, (d) 130 nm and (e) 200 nm. The roughnesses vary from 0.4 to 3.4 nm.

3.2.2 Al-doped zinc oxide grown on titanium nitride films

We deposited aluminum-doped zinc oxide on optically thick TiN films using pulsed laser deposition (PLD) with a 2% AZO target at a temperature of 120°C. We grew film thicknesses spanning from 27 to 63 nanometers. The 27-43 nm films are grown on 60 nm TiN, and the 57 and 63 nm films are grown on 130 nm TiN. For the dielectric functions of AZO, we used a Drude-Lorentz model with a single Lorentz oscillator. Table 5 contains the full model parameters. Figure 11 shows the optical properties of the fabricated AZO films.

Table 5 The Drude-Lorentz Parameters of AZO Films on TiN vs. AZO thickness

Thickness	27 nm	34 nm	45 nm	57 nm	63 nm
A_0	1.619	1.990	2.205	2.519	2.64
B_0	0.210	0.164	0.149	0.146	0.135
A_1	9.794	16.502	18.700	21.544	7.412
B_1	0.005	0.006	0.050	0.006	0.019
E_1	4.143	4.368	4.282	4.386	4.258
ϵ_∞	2.392	2.392	2.264	2.392	3.224
MSE	16.64	22.18	31.84	24.89	22.29

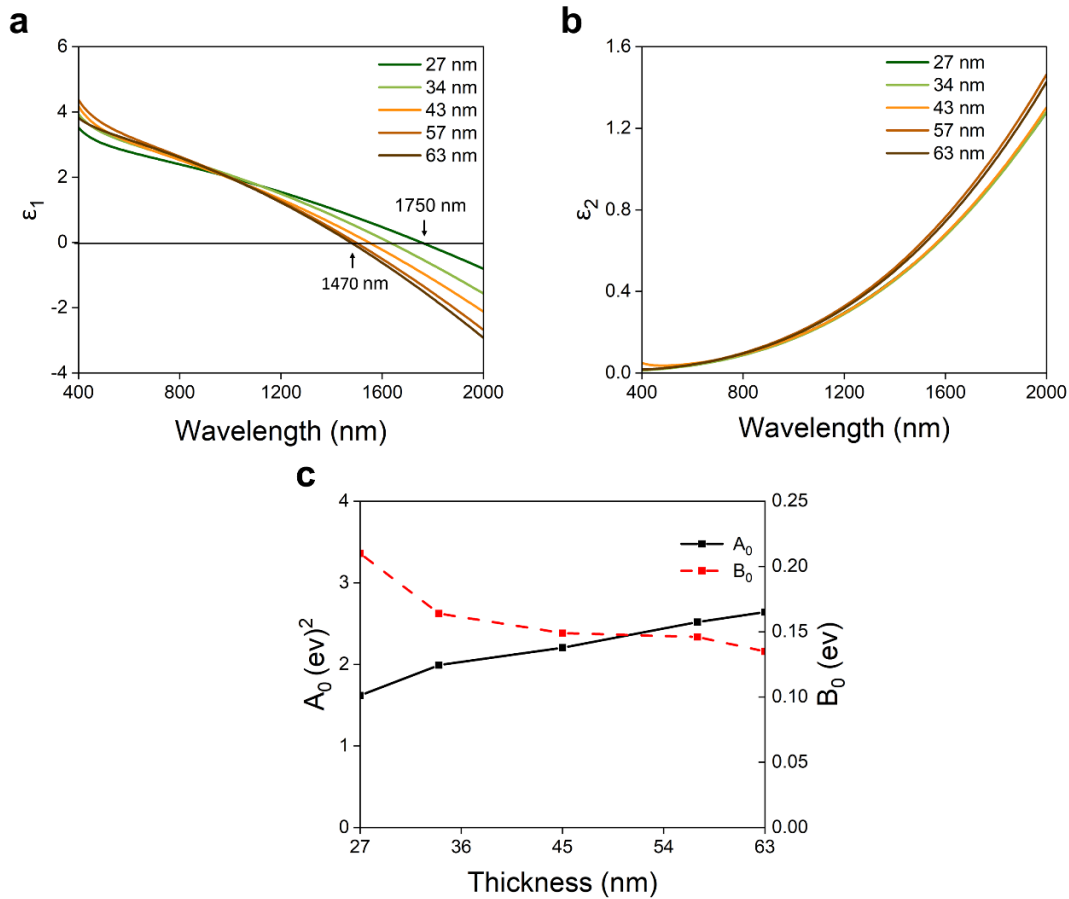


Figure 11 (a)Real part of permittivity of AZO on TiN vs thickness (b)Imaginary permittivity of AZO vs thickness (c)Plasma frequency (A_0) and Drude damping factor (B_0) vs thickness

The ENZ points of the films show a strong blue shift with increasing thicknesses, starting from 1750 nm for the 27-nm-thick films, and reaching the lowest value of 1470 nm for the 63-nm-thick film. The optical losses increase with thickness up to 57 nm then start to saturate for higher thicknesses. With the increasing thickness, the size of the crystalline domains increases, as seen from atomic force microscopy study (Figure 12). Thinner films also have more surface defects that can trap electrons and decrease the carrier concentration. As a result, the carrier concentration increases with increasing thickness¹⁵⁸, and so does the plasma frequency (Fig. 11c)^{159–161}. The thicker films have larger grain sizes with a lower surface-to-volume ratio that decreases the scattering channels for electrons¹⁵⁸. Similar increases in the carrier density and the Hall-mobility with increasing thicknesses of AZO have been observed via conductivity studies for transparent electrode applications by Luka et al¹⁵⁸. Overall, the thicker films are more metallic and the ENZ frequency blueshifts with increasing thickness. The losses increase with the thickness because of

the increasing carrier densities, increasing the plasma frequency but the losses corresponding to the ENZ points decreases with increasing thickness, because of the blue-shifted ENZ.

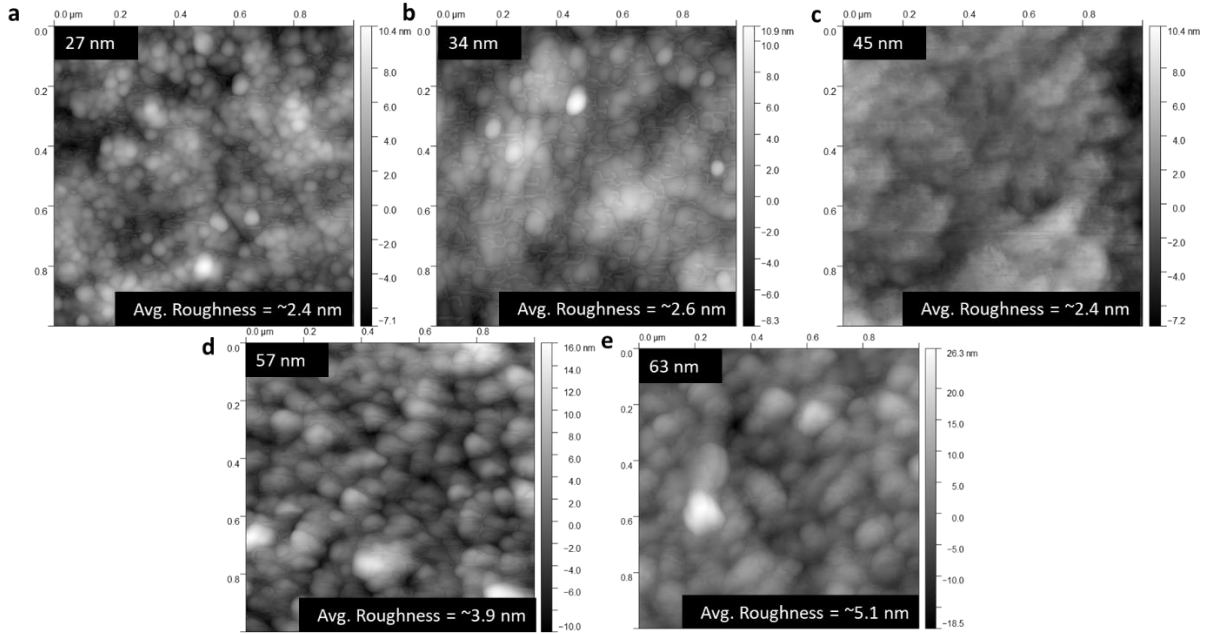


Figure 12 AFM image of AZO films of thickness (a) 27nm, (b) 34 nm, (c) 45 nm, (d) 57 nm and (e) 63 nm, grown on TiN, showing the increasing grain sizes with thickness

3.3 Tailoring AZO-TiN Bilayers for Near Perfect Absorption

We utilize the thickness-tailorable ENZ points of the conducting films to develop wavelength-selective absorbers. In the epsilon-near-zero regime, materials have diminishingly small dielectric permittivity that causes various singularities in their optical responses¹⁶². In this region, strong light-matter interactions induced by slow-light effects and field-intensity enhancement have enabled applications in nonlinearity enhancement^{14,15,19}, femtosecond optical switching^{16,163}, time refraction^{17,46,164}, optical time reversal⁴⁵, and extracting hot electron dynamics in materials¹⁶⁵. Ultrathin ENZ films demonstrate unique absorption resonances for p-polarized light in their ENZ region, termed the Ferrell-Berremann (FB) modes and the ENZ modes. As the film thickness decreases, the bound surface modes on the upper and the lower interface of the film start interacting with each other, hybridizing into symmetric and antisymmetric modes¹⁶⁶. Eventually, the symmetric mode forms a flat dispersion band near the ENZ frequency as the thickness is further reduced. This bound resonance is called the ENZ-mode^{167,168}. The radiative modes called the

Ferrell-Berremann modes are situated in the radiative region occur due to the plasma oscillations in metallic films^{25,169}, and the excitation of the longitudinal optical phonon in dielectric films¹⁷⁰. FB resonances have the further advantage of direct excitation from free space without the need for an additional structure enabling low-cost, lithography-free fabrication. ITO¹¹, CdO¹¹⁹ and AZO³⁴ have been recently utilized in applications such as broadband absorption and polarization switching.

A FB resonator comprises two parts - a robust back-reflector, and an ENZ thin film. The resonance wavelength of the FB metasurface depends on the optical properties of the ENZ film. The TiN-AZO bilayer stacks form a double-resonant FB device, with two dips near the ENZ regions of TiN and AZO for p-polarized light at an angle of incidence of 50 degrees (Fig. 3a). As the AZO ENZ point shows a large variance with the changing thickness, the FB dip at the telecom frequencies can be tailored by changing the thickness of the AZO films. Near these ENZ points, the loss (imaginary permittivity) is around 0.6. Near the telecommunication wavelength, the reflectance spectrum for s-polarized light is flat.

The AZO layer is almost transparent in the visible wavelengths and the structure can be simplified to a thin TiN layer on a reflective silicon substrate. The TiN ENZ point shows a smaller variance (<10nm) with the changing thickness. It has larger losses (imaginary part of the permittivity around 3), resulting in a broad FB dip near 480 nm that is not affected by changing the TiN thickness (Fig. 13b). On the other hand, near the visible wavelengths, s-polarized light shone on TiN shows strong shifts with the thickness variance, indicating the excitation of Fabry-Pérot mode (Fig. 13c). This approach shows how utilizing multilayer stacks and engineering their properties individually can be used to tune the broadband characteristics of the overall structure.

Previously, lithography-free absorbers have been studied for a variety of applications spanning colors¹⁷¹⁻¹⁷³, electrical modulators¹⁷⁴, and polarization switches¹¹⁶. To examine the efficacy of the grown films for use in absorbers, we investigated the effect of the angle of incidence on the spectrum theoretically using a Transfer Matrix Method (TMM) model¹⁷⁵, using the experimentally obtained dielectric properties of the thin films. Figure 3d shows the absorption of the films with respect to the angle of incidence and wavelength. The films show near-perfect absorption around the ENZ region for the larger angle of incidences. The peaks get narrower as the thickness

increases because of decreasing losses, desirable for switching applications. Since the absorption is directly related to the intensity enhancement, shown in prior studies by Anopchenko and Gurung et al.^{176,177}, it would be possible to observe high field intensities inside the AZO film, with potential applications in nonlinear optics spanning time refraction¹⁷⁸, and optical time-reversal¹⁷⁹, and high-harmonic generation¹⁸⁰ using robust ENZ films.

The depth and the quality factor of the resonances depend on many factors in addition to the material losses, such as the angle of incidence, thickness, and the backreflector. As the angle increases the coupling strength to FB modes increases, therefore increasing the attainable maximum absorption¹⁶⁷. Also, lower losses around the ENZ correspond to sharper peaks with both narrower features and higher maximum values. Thicker AZO films have their ENZ frequency at lower wavelengths, with smaller losses. Hence, perfect absorption is attainable with thicker films at larger angles of incidences.

Since the absorptive losses are intrinsic to the material properties, they are expected to be in the same ballpark for AZO grown on different substrates and with different techniques, although slight improvements are expected for epitaxial films. However, even with these losses, epsilon-near-zero enhanced effects such as large reflectance modulation¹⁸¹, frequency translation⁹², addition of nonlinearities¹⁸², and negative refraction¹⁸³ are achievable. Thickness-tailoring provides an additional method of achieving such effects at different wavelengths, which is highlighted in this paper, with the dynamic reflectance modulation as an example.

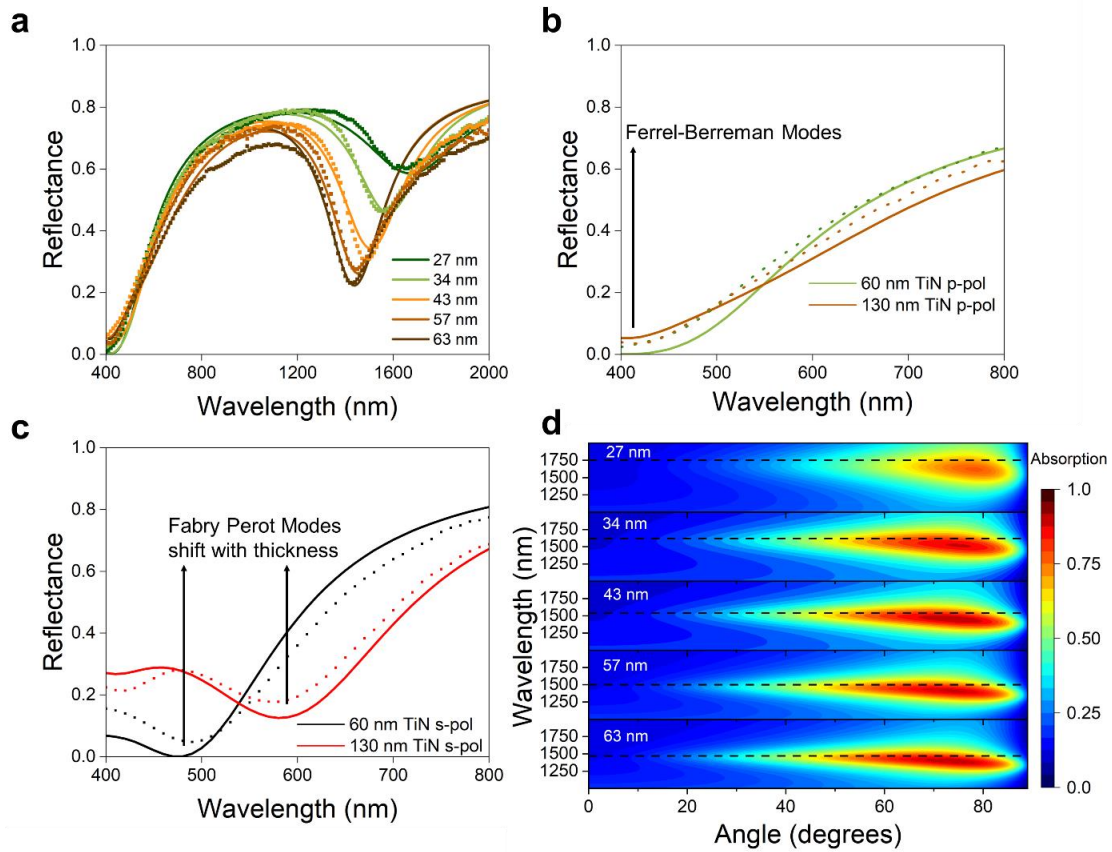


Figure 13 (a) Reflectance spectrum of the ultra-subwavelength AZO on TiN for p-polarized light. (b) Ferrell-Berremann modes for p-polarized and (c) Fabry-Pérot modes for s-polarized light on the TiN-AZO films with varying TiN thickness. The solid lines in a-c are simulation results. The dashed lines are experimental results (d) Angle and Wavelength Dependent Absorption Spectrum of the AZO films obtained using the TMM method

3.4 Dynamic Properties of TiN-AZO bilayers

For a proof-of-concept demonstration of the as-grown films in photonic time-varying applications, we investigated the reflectance modulation of the 63-nm-thick AZO FB absorber with an interband pump – near-infrared (NIR) probe configuration. The pump at 325 nm wavelength is generated by passing a 70 fs, 800 nm pump laser through an OPA. The probe is generated by passing the pump through a sapphire crystal to generate a NIR supercontinuum probe. The pump is at normal incidence, while the probe is at an angle of incidence of 50-degrees (Fig. 14a). Upon excitation by the pump, free carriers generated in the AZO cause the ENZ to blue-shift, resulting in broadband modulation of the reflectance spectrum. As the reflectance spectrum blue shifts due to decreasing refractive index, a positive change is seen to the blue end of the reflectance minimum, and a

negative change is seen at the longer wavelengths. A reflectance change of 15% is seen at 1350 nm, at a pump fluence of 1.5 mJ/cm^2 . The relaxation time of the switching here is on the picosecond scale, with 90% of the signal decaying under 10 ps due to defect-assisted Shockley-Read-Hall mechanisms^{16,184}, after which the modulation is dominated by slower, thermal effects (Fig. 14b,c)¹⁸⁵. Active permittivity modulation of AZO with an applied optical pump may be useful for all-optical transistors¹⁸² and other time-varying metasurface applications^{92,178,186}. Deeper and faster modulation may be possible employing intraband pumps working at larger angles near the FB resonance^{107,187}, enabling stronger pump absorption.

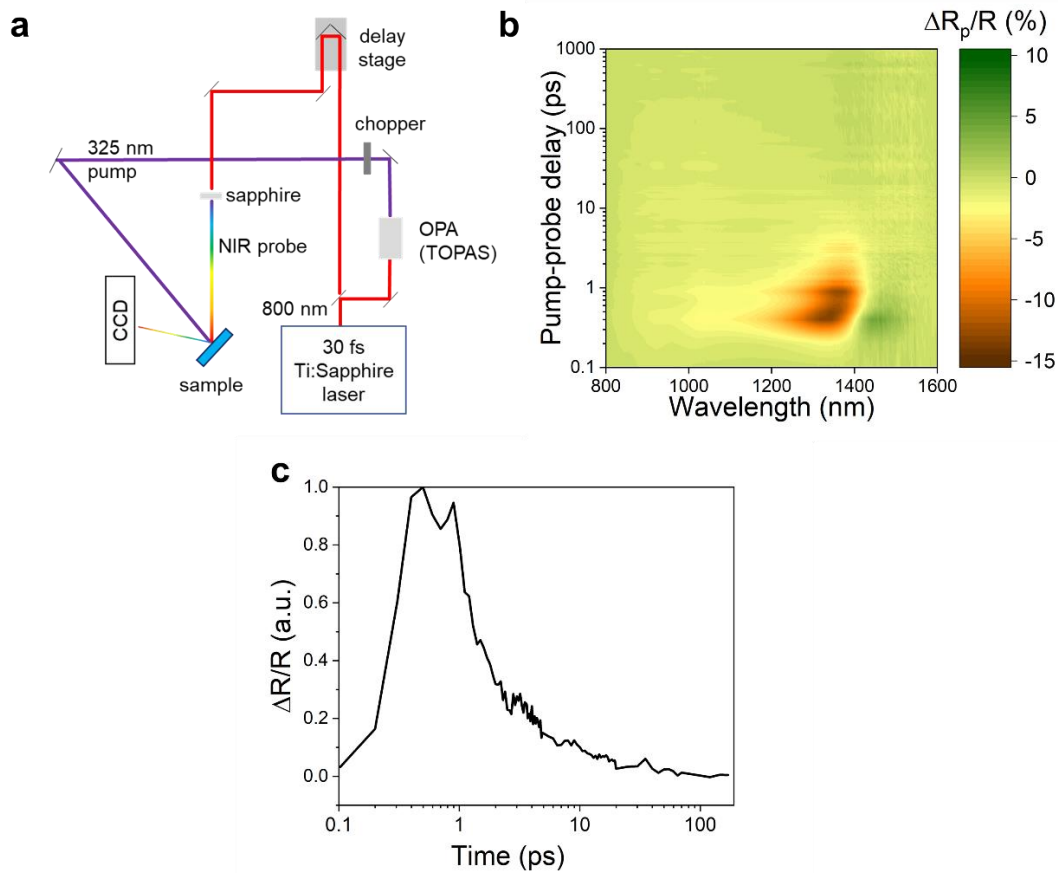


Figure 14 (a) Schematic of the pump-probe setup (b) Color plot showing the reflectance modulation at a pump fluence of 1.5 mJ/cm^2 , at near infrared wavelengths (horizontal axis) versus time (vertical axis). (c) 90% of the signal decays under 10 ps, after which the relaxation is taken over by slower dynamics of the backreflectors. The plot shows the dynamics at a probe wavelength of 1350 nm.

3.5 Chapter Summary

In this work, we investigate the thickness-dependent optical response of conducting nitrides and oxides, namely, plasmonic titanium nitride and aluminum-doped zinc oxide as a tailorable, industry-compatible, low-loss platform for passive and dynamic photonics. Specifically, we study the properties of low-loss, optical grade titanium nitride grown on the technologically relevant silicon substrate. The studied TiN films exhibit plasmonic properties that are better than any previously reported work of TiN on silicon, and in some instances, even better than epitaxial titanium nitride grown at lower temperatures. For both TiN and AZO, we demonstrate that by controlling the thickness, the optical properties of the conducting films can be adjusted. For photonic device demonstrations, we grow aluminum-doped zinc oxide on the as-grown titanium nitride films. Furthermore, we show that the spectral window of the ENZ regime of the studied AZO films can be varied by almost 400 nm by changing the film thickness by ~40 nm, resulting in tailorable Ferrell-Berremann modes spanning the telecommunication wavelength range. Subsequently, we demonstrate strong absorbers utilizing the proposed AZO/TiN bilayers that employ dual Ferrell-Berremann modes, one near the ENZ point of TiN and the other near that of the AZO film. To explore the feasibility of the materials for dynamic photonics, we demonstrate reflectance modulation in the studied AZO/TiN bilayers with pump-probe spectroscopy and show that the absorbance can be tuned at picosecond timescales in the near-infrared range. Since the FB mode only occurs for p-polarized light switching, this can enable active polarization control of the reflected light.

The thickness-dependent optical properties of low-loss conducting films can be employed to develop efficient, tailorable photonic devices including lithography-free light absorbers in the near-infrared to the mid-infrared regime, all-optical switches as well as nonlinear structures for high-harmonic generation.

4. SUMMARY

Temporally modified optical medium is an important key in many research areas including photonic circuitry and optical modulators. Additionally, the new excitement around the time varying media makes it crucial to obtain strong and fast optical switching. Throughout my masters I have worked with ENZ materials investigating this problem. We have considered the problem both in a theoretical way to better illuminate the ENZ switching for experiments and also investigated the material properties for better realization. In the first part, various all-optical switching schemes were explored, particularly the strength of the modulations and their trend in ENZ region with respect to wavelength is considered. We have tried to simplify the process of extracting the material properties from the modulated reflection and transmission data. In the second part, the thickness dependent optical properties of novel plasmonic materials, titanium nitride and aluminum zinc oxide, are investigated. The ENZ region of AZO is controlled over a 300 nm range with 40 nm change in thickness. We have shown in a proof-of-concept-design that ENZ applications can be tuned to cover the telecom range. Additionally, optically high quality polycrystalline TiN films are obtained. The results of these projects will further the knowledge and methods in optical switching and ENZ applications.

REFERENCES

- (1) Schuller, J. A.; Barnard, E. S.; Cai, W.; Jun, Y. C.; White, J. S.; Brongersma, M. L. Plasmonics for Extreme Light Concentration and Manipulation. *Nature Materials* 2010 9:3 **2010**, 9 (3), 193–204. <https://doi.org/10.1038/nmat2630>.
- (2) Gramotnev, D. K.; Bozhevolnyi, S. I. Plasmonics beyond the Diffraction Limit. *Nature Photonics* 2010 4:2 **2010**, 4 (2), 83–91. <https://doi.org/10.1038/nphoton.2009.282>.
- (3) Shcherbakov, M. R.; Vabishchevich, P. P.; Shorokhov, A. S.; Chong, K. E.; Choi, D. Y.; Staude, I.; Miroshnichenko, A. E.; Neshev, D. N.; Fedyanin, A. A.; Kivshar, Y. S. Ultrafast All-Optical Switching with Magnetic Resonances in Nonlinear Dielectric Nanostructures. *Nano Letters* **2015**, 15 (10), 6985–6990. https://doi.org/10.1021/ACS.NANOLETT.5B02989/SUPPL_FILE/NL5B02989_SI_001.PDF.
- (4) Krasnok, A. E.; Evlyukhin, A. B.; Chichkov, B. N.; Baranov, D. G.; Zuev, D. A.; Kotov, O. v.; Lepeshov, S. I. All-Dielectric Nanophotonics: The Quest for Better Materials and Fabrication Techniques. *Optica, Vol. 4, Issue 7, pp. 814-825* **2017**, 4 (7), 814–825. <https://doi.org/10.1364/OPTICA.4.000814>.
- (5) Silveirinha, M.; Engheta, N. Tunneling of Electromagnetic Energy through Subwavelength Channels and Bends Using ϵ -near-Zero Materials. *Physical Review Letters* **2006**, 97 (15). <https://doi.org/10.1103/PhysRevLett.97.157403>.
- (6) Silveirinha, M. G.; Engheta, N. Theory of Supercoupling, Squeezing Wave Energy, and Field Confinement in Narrow Channels and Tight Bends Using ϵ near-Zero Metamaterials. *Physical Review B - Condensed Matter and Materials Physics* **2007**, 76 (24), 245109. <https://doi.org/10.1103/PHYSREVB.76.245109/FIGURES/14/MEDIUM>.
- (7) Liberal, I.; Mahmoud, A. M.; Li, Y.; Edwards, B.; Engheta, N. Photonic Doping of Epsilon-near-Zero Media. *Science (1979)* **2017**, 355 (6329), 1058–1062. https://doi.org/10.1126/SCIENCE.AAL2672/SUPPL_FILE/LIBERAL.SM.PDF.
- (8) Kim, J.; Dutta, A.; Naik, G. v.; Giles, A. J.; Bezares, F. J.; Ellis, C. T.; Tischler, J. G.; Mahmoud, A. M.; Caglayan, H.; Glembocki, O. J.; Kildishev, A. v.; Caldwell, J. D.; Boltasseva, A.; Engheta, N. Role of Epsilon-near-Zero Substrates in the Optical Response of Plasmonic Antennas. *Optica* **2016**, 3 (3), 339. <https://doi.org/10.1364/optica.3.000339>.

- (9) Rensberg, J.; Zhou, Y.; Richter, S.; Wan, C.; Zhang, S.; Schöppe, P.; Schmidt-Grund, R.; Ramanathan, S.; Capasso, F.; Kats, M. A.; Ronning, C. Epsilon-Near-Zero Substrate Engineering for Ultrathin-Film Perfect Absorbers. **2017**. <https://doi.org/10.1103/PhysRevApplied.8.014009>.
- (10) Luk, T. S.; Campione, S.; Kim, I.; Feng, S.; Jun, Y. C.; Liu, S.; Wright, J. B.; Brener, I.; Catrysse, P. B.; Fan, S.; Sinclair, M. B. Directional Perfect Absorption Using Deep Subwavelength Low-Permittivity Films. *PHYSICAL REVIEW B* **2014**, *90*, 85411. <https://doi.org/10.1103/PhysRevB.90.085411>.
- (11) Yoon, J.; Zhou, M.; Badsha, Md. A.; Kim, T. Y.; Jun, Y. C.; Hwangbo, C. K. Broadband Epsilon-Near-Zero Perfect Absorption in the Near-Infrared. *Scientific Reports* **2015**, *5*:1 **2015**, *5* (1), 1–8. <https://doi.org/10.1038/srep12788>.
- (12) Boyd, R. W. Material Slow Light and Structural Slow Light: Similarities and Differences for Nonlinear Optics [Invited]. *JOSA B, Vol. 28, Issue 12, pp. A38-A44* **2011**, *28* (12), A38–A44. <https://doi.org/10.1364/JOSAB.28.000A38>.
- (13) Khurgin, J. B. Slow Light in Various Media: A Tutorial. *Advances in Optics and Photonics, Vol. 2, Issue 3, pp. 287-318* **2010**, *2* (3), 287–318. <https://doi.org/10.1364/AOP.2.000287>.
- (14) Alam, M. Z.; de Leon, I.; Boyd, R. W. Large Optical Nonlinearity of Indium Tin Oxide in Its Epsilon-near-Zero Region. *Science (1979)* **2016**, *352* (6287), 795–797. <https://doi.org/10.1126/science.aae0330>.
- (15) Caspani, L.; Kaipurath, R. P. M.; Clerici, M.; Ferrera, M.; Roger, T.; Kim, J.; Kinsey, N.; Pietrzyk, M.; di Falco, A.; Shalaev, V. M.; Boltasseva, A.; Faccio, D. Enhanced Nonlinear Refractive Index in ϵ -Near-Zero Materials. *Physical Review Letters* **2016**, *116* (23), 1–5. <https://doi.org/10.1103/PhysRevLett.116.233901>.
- (16) Kinsey, N.; DeVault, C.; Kim, J.; Ferrera, M.; Shalaev, V. M.; Boltasseva, A. Epsilon-near-Zero Al-Doped ZnO for Ultrafast Switching at Telecom Wavelengths. *Optica* **2015**, *2* (7), 616. <https://doi.org/10.1364/optica.2.000616>.
- (17) Zhou, Y.; Alam, M. Z.; Karimi, M.; Upham, J.; Reshef, O.; Liu, C.; Willner, A. E.; Boyd, R. W. Broadband Frequency Translation through Time Refraction in an Epsilon-near-Zero Material. *Nature Communications* **2020**, *11* (1), 1–7. <https://doi.org/10.1038/s41467-020-15682-2>.

- (18) Liu, C.; Alam, M. Z.; Pang, K.; Manukyan, K.; Reshef, O.; Zhou, Y.; Choudhary, S.; Patrow, J.; Pennathurs, A.; Song, H.; Zhao, Z.; Zhang, R.; Alishahi, F.; Fallahpour, A.; Cao, Y.; Almainan, A.; Dawlaty, J. M.; Tur, M.; Boyd, R. W.; Willner, A. E. Photon Acceleration Using a Time-Varying Epsilon-near-Zero Metasurface. **2021**, *39*, 32. <https://doi.org/10.1021/acsp Photonics.0c01929>.
- (19) Capretti, A.; Negro, L. D.; Engheta, N.; Wang, Y. Enhanced Third-Harmonic Generation in Si-Compatible Epsilon-near-Zero Indium Tin Oxide Nanolayers. *Optics Letters*, Vol. 40, Issue 7, pp. 1500-1503 **2015**, *40* (7), 1500–1503. <https://doi.org/10.1364/OL.40.001500>.
- (20) Luk, T. S.; de Ceglia, D.; Liu, S.; Keeler, G. A.; Prasankumar, R. P.; Vincenti, M. A.; Scalora, M.; Sinclair, M. B.; Campione, S. Enhanced Third Harmonic Generation from the Epsilon-near-Zero Modes of Ultrathin Films. *Applied Physics Letters* **2015**, *106* (15). <https://doi.org/10.1063/1.4917457>.
- (21) Rodríguez-Suné, L.; Scalora, M.; Johnson, A. S.; Cojocar, C.; Akozbek, N.; Coppens, Z. J.; Perez-Salinas, D.; Wall, S.; Trull, J. Study of Second and Third Harmonic Generation from an Indium Tin Oxide Nanolayer: Influence of Nonlocal Effects and Hot Electrons. *APL Photonics* **2020**, *5*, 10801. <https://doi.org/10.1063/1.5129627>.
- (22) Yang, Y.; Lu, J.; Manjavacas, A.; Luk, T. S.; Liu, H.; Kelley, K.; Maria, J.-P.; Runnerstrom, E. L.; Sinclair, M. B.; Ghimire, S.; Brener, I. High-Harmonic Generation from an Epsilon-near-Zero Material. *Nature Physics*. <https://doi.org/10.1038/s41567-019-0584-7>.
- (23) Argyropoulos, C.; Chen, P.-Y.; Aguanno, G. D. ’; Engheta, N.; Ai, A. Boosting Optical Nonlinearities In-near-Zero Plasmonic Channels. *PHYSICAL REVIEW B* **2012**, *85*, 45129. <https://doi.org/10.1103/PhysRevB.85.045129>.
- (24) Maas, R.; Parsons, J.; Engheta, N.; Polman, A. Experimental Realization of an Epsilon-near-Zero Metamaterial at Visible Wavelengths. *Nature Photonics* *2013 7:11* **2013**, *7* (11), 907–912. <https://doi.org/10.1038/nphoton.2013.256>.
- (25) Newman, W. D.; Cortes, C. L.; Atkinson, J.; Pramanik, S.; DeCorby, R. G.; Jacob, Z. Ferrell–Berreman Modes in Plasmonic Epsilon-near-Zero Media. *ACS Photonics* **2014**, *2* (1), 2–7. <https://doi.org/10.1021/PH5003297>.
- (26) Li, Y.; Kita, S.; Muñoz, P.; Reshef, O.; Vulis, D. I.; Yin, M.; Lončar, M.; Mazur, E. On-Chip Zero-Index Metamaterials. *Nature Photonics* *2015 9:11* **2015**, *9* (11), 738–742. <https://doi.org/10.1038/nphoton.2015.198>.

- (27) Li, W.; Guler, U.; Kinsey, N.; Naik, G. v.; Boltasseva, A.; Guan, J.; Shalaev, V. M.; Kildishev, A. v. Refractory Plasmonics with Titanium Nitride: Broadband Metamaterial Absorber. *Advanced Materials* **2014**, *26* (47), 7959–7965. <https://doi.org/10.1002/ADMA.201401874>.
- (28) Naik, G. v.; Schroeder, J. L.; Ni, X.; Kildishev, A. v.; Sands, T. D.; Boltasseva, A. Titanium Nitride as a Plasmonic Material for Visible and Near-Infrared Wavelengths. *Optical Materials Express*, *Vol. 2, Issue 4*, pp. 478-489 **2012**, *2* (4), 478–489. <https://doi.org/10.1364/OME.2.000478>.
- (29) Boltasseva, A.; Atwater, H. A. Low-Loss Plasmonic Metamaterials. *Science (1979)* **2011**, *331* (January), 290–292.
- (30) Naik, G. v.; Kim, J.; Boltasseva, A. Oxides and Nitrides as Alternative Plasmonic Materials in the Optical Range [Invited]. *Optical Materials Express* **2011**, *1* (6), 1090. <https://doi.org/10.1103/PhysRevLett.107.133901>.
- (31) Kinsey, N.; DeVault, C.; Kim, J.; Ferrera, M.; Shalaev, V. M.; Boltasseva, A. A. Epsilon-near-Zero Al-Doped ZnO for Ultrafast Switching at Telecom Wavelengths. *Optica* **2015**, *2* (7), 616. <https://doi.org/10.1364/optica.2.000616>.
- (32) Clerici, M.; Kinsey, N.; DeVault, C.; Kim, J.; Carnemolla, E. G.; Caspani, L.; Shaltout, A.; Faccio, D.; Shalaev, V.; Boltasseva, A.; Ferrera, M. Controlling Hybrid Nonlinearities in Transparent Conducting Oxides via Two-Colour Excitation. *Nat Commun* **2017**, *8* (1), 15829. <https://doi.org/10.1038/ncomms15829>.
- (33) Yang, Y.; Kelley, K.; Sachet, E.; Campione, S.; Luk, T. S.; Maria, J. P.; Sinclair, M. B.; Brener, I. Femtosecond Optical Polarization Switching Using a Cadmium Oxide-Based Perfect Absorber. *Nature Photonics* **2017**, *11* (6), 390–395. <https://doi.org/10.1038/nphoton.2017.64>.
- (34) Gurung, S.; Anopchenko, A.; Bej, S.; Joyner, J.; Myers, J. D.; Frantz, J.; Lee, H. W. H. Atomic Layer Engineering of Epsilon-Near-Zero Ultrathin Films with Controllable Field Enhancement. *Advanced Materials Interfaces* **2020**, *7* (17). <https://doi.org/10.1002/admi.202000844>.

- (35) Saha, S.; Diroll, B. T.; Shank, J.; Kudyshev, Z.; Dutta, A.; Chowdhury, S. N.; Luk, T. S.; Campione, S.; Schaller, R. D.; Shalaev, V. M.; Boltasseva, A.; Wood, M. G. Broadband, High-Speed, and Large-Amplitude Dynamic Optical Switching with Yttrium-Doped Cadmium Oxide. *Advanced Functional Materials* **2020**, *30* (7), 1908377. <https://doi.org/10.1002/adfm.201908377>.
- (36) Zhao, H.; Wang, Y.; Capretti, A.; Dal Negro, L.; Klamkin, J. Broadband Electroabsorption Modulators Design Based on Epsilon-near-Zero Indium Tin Oxide. *IEEE Journal of Selected Topics in Quantum Electronics* **2015**, *21* (4), 192–198. <https://doi.org/10.1109/JSTQE.2014.2375153>.
- (37) Cleary, J. W.; Smith, E. M.; Leedy, K. D.; Grzybowski, G.; Guo, J. Optical and Electrical Properties of Ultra-Thin Indium Tin Oxide Nanofilms on Silicon for Infrared Photonics. *Optical Materials Express* **2018**, *8* (5), 1231. <https://doi.org/10.1364/ome.8.001231>.
- (38) Wang, Y.; Overvig, A. C.; Shrestha, S.; Zhang, R.; Wang, R.; Yu, N.; Dal Negro, L. Tunability of Indium Tin Oxide Materials for Mid-Infrared Plasmonics Applications. *Optical Materials Express* **2017**, *7* (8), 2727. <https://doi.org/10.1364/ome.7.002727>.
- (39) Abb, M.; Albella, P.; Aizpurua, J.; Muskens, O. L. All-Optical Control of a Single Plasmonic Nanoantenna - ITO Hybrid. *Nano Letters* **2011**, *11* (6), 2457–2463. <https://doi.org/10.1021/nl200901w>.
- (40) Wu, J.; Xie, Z. T.; Fu, H. Y.; Li, Q. High-Order Harmonic Generations in Epsilon-Near-Zero Aluminum-Doped Zinc Oxide Nanopyramid Array. *2020 12th International Conference on Advanced Infocomm Technology, ICAIT 2020* **2020**, No. 2, 5–9. <https://doi.org/10.1109/ICAIT51223.2020.9315419>.
- (41) Tian, W.; Liang, F.; Lu, D.; Yu, H.; Zhang, H. Highly Efficient Ultraviolet High-Harmonic Generation from Epsilon-near-Zero Indium Tin Oxide Films. *Photonics Research* **2021**, *9* (3), 317. <https://doi.org/10.1364/prj.414570>.
- (42) DeVault, C.; Zenin, V. A.; Pors, A.; Kim, J.; Chaudhuri, K.; Bozhevolnyi, S.; Shalaev, V. M.; Boltasseva, A. Plasmonic Antenna Resonance Pinning and Suppression of Near-Field Coupling from Epsilon-near-Zero Substrate. *2017 Conference on Lasers and Electro-Optics, CLEO 2017 - Proceedings* **2017**, 2017-Janua, 1–2. https://doi.org/10.1364/CLEO_QELS.2017.FTu4H.5.

- (43) DeVault, C. T.; Zenin, V. A.; Pors, A.; Chaudhuri, K.; Kim, J.; Boltasseva, A.; Shalaev, V. M.; Bozhevolnyi, S. I. Suppression of Near-Field Coupling in Plasmonic Antennas on Epsilon-near-Zero Substrates. *Optica* **2018**, *5* (12), 1557. <https://doi.org/10.1364/optica.5.001557>.
- (44) Schulz, S. A.; Tahir, A. A.; Alam, M. Z.; Upham, J.; de Leon, I.; Boyd, R. W. Optical Response of Dipole Antennas on an Epsilon-near-Zero Substrate. *Physical Review A* **2016**, *93* (6), 1–4. <https://doi.org/10.1103/PhysRevA.93.063846>.
- (45) Vezzoli, S.; Bruno, V.; DeVault, C.; Roger, T.; Shalaev, V. M.; Boltasseva, A.; Ferrera, M.; Clerici, M.; Dubietis, A.; Faccio, D. Optical Time Reversal from Time-Dependent Epsilon-Near-Zero Media. *Physical Review Letters* **2018**, *120* (4), 43902. <https://doi.org/10.1103/PhysRevLett.120.043902>.
- (46) Khurgin, J. B.; Clerici, M.; Bruno, V.; Caspani, L.; DeVault, C.; Kim, J.; Shaltout, A.; Boltasseva, A.; Shalaev, V. M.; Ferrera, M.; Faccio, D.; Kinsey, N. Adiabatic Frequency Shifting in Epsilon-near-Zero Materials: The Role of Group Velocity. *Optica* **2020**, *7* (3), 226. <https://doi.org/10.1364/optica.374788>.
- (47) Pang, K.; Alam, M. Z.; Zhou, Y.; Liu, C.; Reshef, O.; Manukyan, K.; Voegtle, M.; Pennathur, A.; Tseng, C.; Su, X.; Song, H.; Zhao, Z.; Zhang, R.; Song, H.; Hu, N.; Almaiman, A.; Dawlaty, J. M.; Boyd, R. W.; Tur, M.; Willner, A. E. Adiabatic Frequency Conversion Using a Time-Varying Epsilon-Near-Zero Metasurface. *Nano Letters* **2021**, *21* (14), 5907–5913. <https://doi.org/10.1021/acs.nanolett.1c00550>.
- (48) Zhou, Y.; Alam, M. Z.; Karimi, M.; Upham, J.; Reshef, O.; Liu, C.; Willner, A. E.; Boyd, R. W. Broadband Frequency Translation through Time Refraction in an Epsilon-near-Zero Material. *Nature Communications* **2020**, *11* (1), 2180. <https://doi.org/10.1038/s41467-020-15682-2>.
- (49) Bruno, V.; DeVault, C.; Vezzoli, S.; Kudyshev, Z.; Huq, T.; Mignuzzi, S.; Jacassi, A.; Saha, S.; Shah, Y. D.; Maier, S. A.; Cumming, D. R. S.; Boltasseva, A.; Ferrera, M.; Clerici, M.; Faccio, D.; Sapienza, R.; Shalaev, V. M. Negative Refraction in Time-Varying Strongly Coupled Plasmonic-Antenna–Epsilon-Near-Zero Systems. *Physical Review Letters* **2020**, *124* (4), 043902. <https://doi.org/10.1103/PhysRevLett.124.043902>.
- (50) Lustig, E.; Sharabi, Y.; Segev, M. Topological Aspects of Photonic Time Crystals. *Optica* **2018**, *5* (11), 1390. <https://doi.org/10.1364/optica.5.001390>.

- (51) Kinsey, N.; DeVault, C.; Boltasseva, A.; Shalaev, V. M. Near-Zero-Index Materials for Photonics. *Nature Reviews Materials*. Nature Research December 1, 2019, pp 742–760. <https://doi.org/10.1038/s41578-019-0133-0>.
- (52) Diroll, B. T.; Saha, S.; Shalaev, V. M.; Boltasseva, A.; Schaller, R. D. Broadband Ultrafast Dynamics of Refractory Metals: TiN and ZrN. *Advanced Optical Materials* **2020**, *8* (19). <https://doi.org/10.1002/adom.202000652>.
- (53) Bohn, J.; Luk, T. S.; Tollerton, C.; Hutchings, S. W.; Brener, I.; Horsley, S.; Barnes, W. L.; Hendry, E. All-Optical Switching of an Epsilon-near-Zero Plasmon Resonance in Indium Tin Oxide. *Nature Communications* **2021**, *12* (1). <https://doi.org/10.1038/s41467-021-21332-y>.
- (54) Alam, M. Z.; de Leon, I.; Boyd, R. W. Large Optical Nonlinearity of Indium Tin Oxide in Its Epsilon-near-Zero Region. *Science (1979)* **2016**, *352* (6287), 795–797. <https://doi.org/10.1126/SCIENCE.AAE0330>.
- (55) Saha, S.; Dutta, A.; DeVault, C.; Diroll, B. T.; Schaller, R. D.; Kudyshev, Z.; Xu, X.; Kildishev, A.; Shalaev, V. M.; Boltasseva, A. Extraordinarily Large Permittivity Modulation in Zinc Oxide for Dynamic Nanophotonics. *Materials Today* **2021**, *43*, 27–36. <https://doi.org/10.1016/j.mattod.2020.10.023>.
- (56) Babicheva, V. E.; Boltasseva, A.; Lavrinenko, A. v. Transparent Conducting Oxides for Electro-Optical Plasmonic Modulators. *Nanophotonics* **2015**, *4* (2), 165–185. <https://doi.org/10.1515/NANOPH-2015-0004>.
- (57) Dunkelberger, A. D.; Ratchford, D. C.; Grafton, A. B.; Breslin, V. M.; Ryland, E. S.; Katzer, D. S.; Fears, K. P.; Weiblen, R. J.; Vurgaftman, I.; Giles, A. J.; Ellis, C. T.; Tischler, J. G.; Caldwell, J. D.; Owrutsky, J. C. Ultrafast Active Tuning of the Berreman Mode. *ACS Photonics* **2020**, *7* (1), 279–287. <https://doi.org/10.1021/acsp Photonics.9b01578>.
- (58) Secondo, R.; Khurgin, J.; Kinsey, N. Absorptive Loss and Band Non-Parabolicity as a Physical Origin of Large Nonlinearity in Epsilon-near-Zero Materials. *Optical Materials Express* **2020**, *10* (7), 1545. <https://doi.org/10.1364/ome.394111>.
- (59) Rashed, A. R.; Can Yildiz, B.; Ayyagari, S. R.; Caglayan, H. Hot Electron Dynamics in Ultrafast Multilayer Epsilon-near-Zero Metamaterials. *Physical Review B* **2020**, *101*, 165301. <https://doi.org/10.1103/PhysRevB.101.165301>.

- (60) Wang, H.; Du, K.; Dai, X.; Zhang, W.; Liu, R.; Chua, S. J.; Mei, T. Role of Hot Electron Scattering in Epsilon-near-Zero Optical Nonlinearity. *Nanophotonics* **2020**, *9* (14), 4287–4293. <https://doi.org/10.1515/nanoph-2020-0266>.
- (61) Guo, Q.; Cui, Y.; Yao, Y.; Ye, Y.; Yang, Y.; Liu, X.; Zhang, S.; Liu, X.; Qiu, J.; Hosono, H. A Solution-Processed Ultrafast Optical Switch Based on a Nanostructured Epsilon-Near-Zero Medium. *Advanced Materials* **2017**, *29* (27), 1700754. <https://doi.org/10.1002/adma.201700754>.
- (62) George, H.; Reed, J.; Ferdinandus, M.; DeVault, C.; Lagutchev, A.; Urbas, A.; Norris, T. B.; Shalaev, Vladimir. M.; Boltasseva, A.; Kinsey, N. Nonlinearities and Carrier Dynamics in Refractory Plasmonic TiN Thin Films. *Optical Materials Express* **2019**, *9* (10), 3911. <https://doi.org/10.1364/ome.9.003911>.
- (63) Saleh, B. E. A.; Teich, M. C. *Fundamentals of Photonics*; John Wiley & Sons, 2019.
- (64) Campione, S.; Brener, I.; Marquier, F. Theory of Epsilon-near-Zero Modes in Ultrathin Films. *Physical Review B - Condensed Matter and Materials Physics* **2015**, *91* (12), 1–5. <https://doi.org/10.1103/PhysRevB.91.121408>.
- (65) Campione, S.; Kim, I.; de Ceglia, D.; Keeler, G. A.; Luk, T. S. Experimental Verification of Epsilon-near-Zero Plasmon Polariton Modes in Degenerately Doped Semiconductor Nanolayers. *Optics Express* **2016**, *24* (16), 18782. <https://doi.org/10.1364/oe.24.018782>.
- (66) Meeten, G. H. Refractive Index Errors in the Critical-Angle and the Brewster-Angle Methods Applied to Absorbing and Heterogeneous Materials. *Measurement Science and Technology* **1997**, *8* (7), 728–733. <https://doi.org/10.1088/0957-0233/8/7/006>.
- (67) Kliewer, K. L.; Fuchs, R. Collective Electronic Motion in a Metallic Slab. *Physical Review* **1967**, *153* (2), 498–512. <https://doi.org/10.1103/PhysRev.153.498>.
- (68) Traviss, D.; Bruck, R.; Mills, B.; Abb, M.; Muskens, O. L. Ultrafast Plasmonics Using Transparent Conductive Oxide Hybrids in the Epsilon-near-Zero Regime. *Applied Physics Letters* **2013**, *102* (12), 121112. <https://doi.org/10.1063/1.4798833>.
- (69) Chaudhuri, K.; Guler, U.; Azzam, S. I.; Reddy, H.; Saha, S.; Marinero, E. E.; Kildishev, A. V.; Shalaev, V. M.; Boltasseva, A. Remote Sensing of High Temperatures with Refractory, Direct-Contact Optical Metacavity. *ACS Photonics* **2020**, *7*, 472–479. <https://doi.org/10.1021/acsp Photonics.9b01450>.

- (70) Berini, P. Long-Range Surface Plasmon Polaritons. **2009**.
<https://doi.org/10.1364/AOP.1.000484>.
- (71) Khurgin, J. B.; Clerici, M.; Kinsey, N. Fast and Slow Nonlinearities in Epsilon-Near-Zero Materials. *Laser and Photonics Reviews* **2021**, *15* (2), 2000291.
<https://doi.org/10.1002/lpor.202000291>.
- (72) Khurgin, J. B. Slow Light in Various Media: A Tutorial. *Advances in Optics and Photonics* **2010**, *2* (3), 287. <https://doi.org/10.1364/aop.2.000287>.
- (73) Kinsey, N.; Khurgin, J. Nonlinear Epsilon-near-Zero Materials Explained: Opinion. *Optical Materials Express* **2019**, *9* (7), 2793. <https://doi.org/10.1364/ome.9.002793>.
- (74) Ferrell, R. A. Predicted Radiation of Plasma Oscillations in Metal Films*. *Physical Review* **1958**, *111* (5).
- (75) Berreman, D. W. Infrared Absorption at Longitudinal Optic Frequency in Cubic Crystal Films. *Physical Review* **1963**, *130* (6), 2193–2198.
- (76) Newman, W. D.; Cortes, C. L.; Atkinson, J.; Pramanik, S.; Decorby, R. G.; Jacob, Z. Ferrell-Berreman Modes in Plasmonic Epsilon-near-Zero Media. *ACS Photonics* **2015**, *2* (1), 2–7.
<https://doi.org/10.1021/ph5003297>.
- (77) Park, J.; Kang, J. H.; Liu, X.; Brongersma, M. L. Electrically Tunable Epsilon-Near-Zero (ENZ) Metafilm Absorbers. *Scientific Reports* **2015**, *5* (Mim), 1–9.
<https://doi.org/10.1038/srep15754>.
- (78) Kretschmann, E.; Raether, H. Radiative Decay of Non Radiative Surface Plasmons Excited by Light. *Zeitschrift für Naturforschung A* **1968**, *23* (12), 2135–2136.
- (79) Otto, A.; Burstein, E.; Demartina, F. The Surface Polariton Response in Attenuated Total Reflection. In *Polaritons: Proceedings of the the First Taormina Research Conference on the Structure of Matter*; 1974; pp 117–121.
- (80) Anopchenko, A.; Tao, L.; Arndt, C.; Lee, H. W. H. Field-Effect Tunable and Broadband Epsilon-Near-Zero Perfect Absorbers with Deep Subwavelength Thickness. *ACS Photonics* **2018**, *5* (7), 2631–2637. <https://doi.org/10.1021/acsphotonics.7b01373>.
- (81) Vinogradov, A. P.; Dorofeenko, A. v; Pukhov, A. A.; Lisyansky, A. A. Exciting Surface Plasmon Polaritons in the Kretschmann Configuration by a Light Beam. *Physical Review B* **2018**, *97*, 235407. <https://doi.org/10.1103/PhysRevB.97.235407>.

- (82) Vassant, S.; Hugonin, J.-P.; Marquier, F.; Greffet, J.-J. Berreman Mode and Epsilon near Zero Mode. *Optics Express* **2012**, *20* (21), 23971. <https://doi.org/10.1364/oe.20.023971>.
- (83) Runnerstrom, E. L.; Kelley, K. P.; Sachet, E.; Shelton, C. T.; Maria, J. P. Epsilon-near-Zero Modes and Surface Plasmon Resonance in Fluorine-Doped Cadmium Oxide Thin Films. *ACS Photonics* **2017**, *4* (8), 1885–1892. <https://doi.org/10.1021/acsphotonics.7b00429>.
- (84) Caspani, L.; Kaipurath, R. P. M. M.; Clerici, M.; Ferrera, M.; Roger, T.; Kim, J.; Kinsey, N.; Pietrzyk, M.; Falco, A. di; Shalaev, V. M.; Boltasseva, A.; Faccio, D.; di Falco, A. Enhanced Nonlinear Refractive Index in ϵ -Near-Zero Materials. *Physical Review Letters* **2016**, *116* (23), 1–5. <https://doi.org/10.1103/PhysRevLett.116.233901>.
- (85) Carnemolla, E. G.; Caspani, L.; DeVault, C.; Clerici, M.; Vezzoli, S.; Bruno, V.; Shalaev, V. M.; Faccio, D.; Boltasseva, A.; Ferrera, M. Degenerate Optical Nonlinear Enhancement in Epsilon-near-Zero Transparent Conducting Oxides. *Optical Materials Express* **2018**, *8* (11), 3392. <https://doi.org/10.1364/ome.8.003392>.
- (86) Yang, Y.; Lu, J.; Manjavacas, A.; Luk, T. S.; Liu, H.; Kelley, K.; Maria, J. P.; Runnerstrom, E. L.; Sinclair, M. B.; Ghimire, S.; Brener, I. High-Harmonic Generation from an Epsilon-near-Zero Material. *Nature Physics*. Nature Publishing Group July 15, 2019, pp 1022–1026. <https://doi.org/10.1038/s41567-019-0584-7>.
- (87) Luk, T. S.; Campione, S.; Kim, I.; Feng, S.; Jun, Y. C.; Liu, S.; Wright, J. B.; Brener, I.; Catrysse, P. B.; Fan, S.; Sinclair, M. B. Directional Perfect Absorption Using Deep Subwavelength Low-Permittivity Films. *Physical Review B - Condensed Matter and Materials Physics* **2014**, *90* (8), 1–10. <https://doi.org/10.1103/PhysRevB.90.085411>.
- (88) Rensberg, J.; Zhou, Y.; Richter, S.; Wan, C.; Zhang, S.; Schöppe, P.; Schmidt-Grund, R.; Ramanathan, S.; Capasso, F.; Kats, M. A.; Ronning, C. Epsilon-Near-Zero Substrate Engineering for Ultrathin-Film Perfect Absorbers. *Physical Review Applied* **2017**, *8* (1), 1–11. <https://doi.org/10.1103/PhysRevApplied.8.014009>.
- (89) Puerto, D.; Siegel, J.; Gawelda, W.; Galvan-Sosa, M.; Ehrentraut, L.; Bonse, J.; Solis, J. Dynamics of Plasma Formation, Relaxation, and Topography Modification Induced by Femtosecond Laser Pulses in Crystalline and Amorphous Dielectrics. *Journal of the Optical Society of America B* **2010**, *27* (5), 1065. <https://doi.org/10.1364/josab.27.001065>.

- (90) Kirby, R. J.; Ferrenti, A.; Weinberg, C.; Klemenz, S.; Oudah, M.; Lei, S.; Weber, C. P.; Fausti, D.; Scholes, G. D.; Schoop, L. M. Transient Drude Response Dominates Near-Infrared Pump-Probe Reflectivity in Nodal-Line Semimetals ZrSiS and ZrSiSe. *Journal of Physical Chemistry Letters* **2020**, *11* (15), 6105–6111. <https://doi.org/10.1021/acs.jpcllett.0c01377>.
- (91) Kuttruff, J.; Garoli, D.; Allerbeck, J.; Krahne, R.; de Luca, A.; Brida, D.; Caligiuri, V.; Maccaferri, N. Ultrafast All-Optical Switching Enabled by Epsilon-near-Zero-Tailored Absorption in Metal-Insulator Nanocavities. *Communications Physics* **2020**, *3* (1), 1–7. <https://doi.org/10.1038/s42005-020-0379-2>.
- (92) Bruno, V.; Vezzoli, S.; DeVault, C.; Carnemolla, E.; Ferrera, M.; Boltasseva, A.; Shalaev, V. M.; Faccio, D.; Clerici, M.; de Vault, C.; Carnemolla, E.; Ferrera, M.; Boltasseva, A.; Shalaev, V. M.; Faccio, D.; Clerici, M. Broad Frequency Shift of Parametric Processes in Epsilon-Near-Zero Time-Varying Media. *Applied Sciences* **2020**, *10* (4), 1318. <https://doi.org/10.3390/app10041318>.
- (93) Patsalas, P.; Kalfagiannis, N.; Kassavetis, S. Optical Properties and Plasmonic Performance of Titanium Nitride. *Materials* **2015**, *Vol. 8, Pages 3128-3154* **2015**, *8* (6), 3128–3154. <https://doi.org/10.3390/MA8063128>.
- (94) Park, D. G.; Cha, T. H.; Lim, K. Y.; Cho, H. J.; Kim, T. K.; Jang, S. A.; Suh, Y. S.; Misra, V.; Yeo, I. S.; Roh, J. S.; Park, J. W.; Yoon, H. K. Robust Ternary Metal Gate Electrodes for Dual Gate CMOS Devices. *Technical Digest-International Electron Devices Meeting* **2001**, 671–674. <https://doi.org/10.1109/IEDM.2001.979597>.
- (95) Chang, C.-C.; Nogan, J.; Yang, Z.-P.; Kort-Kamp, W. J. M.; Ross, W.; Luk, T. S.; Dalvit, D. A. R.; Azad, A. K.; Chen, H.-T. Highly Plasmonic Titanium Nitride by Room-Temperature Sputtering. *Scientific Reports* **2019**, *9:1* **2019**, *9* (1), 1–9. <https://doi.org/10.1038/s41598-019-51236-3>.
- (96) Georgson, M.; Roos, A.; Ribbing, C. -G. The Influence of Preparation Conditions on the Optical Properties of Titanium Nitride Based Solar Control Films. *Journal of Vacuum Science & Technology A: Vacuum, Surfaces, and Films* **1998**, *9* (4), 2191. <https://doi.org/10.1116/1.577249>.

- (97) Wang, Y.; Capretti, A.; Dal Negro, L. Wide Tuning of the Optical and Structural Properties of Alternative Plasmonic Materials. *Optical Materials Express* **2015**, *5* (11), 2415. <https://doi.org/10.1364/OME.5.002415>.
- (98) Pasupathi Sugavaneshwar, R.; Ishii, S.; Thang, †; Dao, D.; Ohi, A.; Nabatame, T.; Nagao, T.; Sugavaneshwar, R. P.; Ishii, S.; Dao, T. D.; Ohi, A.; Nabatame, T.; Nagao, T. Fabrication of Highly Metallic TiN Films by Pulsed Laser Deposition Method for Plasmonic Applications. *ACS Photonics* **2018**, *5* (3), 814–819. <https://doi.org/10.1021/acsp Photonics.7b00942>.
- (99) Secondo, R.; Avrutin, V.; Özgür, Ü.; Kinsey, N. Optimization of Titanium Nitride Films Using Plasma Enhanced Atomic Layer Deposition.
- (100) Gui, L.; Bagheri, S.; Strohhfeldt, N.; Hentschel, M.; Zgrabik, C. M.; Metzger, B.; Linnenbank, H.; Hu, E. L.; Giessen, H. Nonlinear Refractory Plasmonics with Titanium Nitride Nanoantennas. *Nano Letters* **2016**, *16* (9), 5708–5713. <https://doi.org/10.1021/acs.nanolett.6b02376>.
- (101) Li, W.; Guler, U.; Kinsey, N.; Naik, G. v.; Boltasseva, A.; Guan, J.; Shalaev, V. M.; Kildishev, A. v. Refractory Plasmonics with Titanium Nitride: Broadband Metamaterial Absorber. *Advanced Materials* **2014**, *26* (47), 7959–7965. <https://doi.org/10.1002/adma.201401874>.
- (102) Chaudhuri, K.; Guler, U.; Azzam, S. I. S. I.; Reddy, H.; Saha, S.; Marinero, E. E. E.; Kildishev, A. V. A. v.; Shalaev, V. M. V. M.; Boltasseva, A. Remote Sensing of High Temperatures with Refractory, Direct-Contact Optical Metacavity. *ACS Photonics* **2020**, *7* (2), 472–479. <https://doi.org/10.1021/acsp Photonics.9b01450>.
- (103) Chirumamilla, M.; Chirumamilla, A.; Yang, Y.; Roberts, A. S.; Kristensen, P. K.; Chaudhuri, K.; Boltasseva, A.; Sutherland, D. S.; Bozhevolnyi, S. I.; Pedersen, K. Large-Area Ultrabroadband Absorber for Solar Thermophotovoltaics Based on 3D Titanium Nitride Nanopillars. *Advanced Optical Materials* **2017**, *5* (22), 1700552. <https://doi.org/10.1002/adom.201700552>.
- (104) Saha, S.; Dutta, A.; Kinsey, N.; Kildishev, A. v.; Shalaev, V. M.; Boltasseva, A. On-Chip Hybrid Photonic-Plasmonic Waveguides with Ultrathin Titanium Nitride Films. *ACS Photonics* **2018**, *5* (11), 4423–4431. <https://doi.org/10.1021/acsp Photonics.8b00885>.

- (105) Kinsey, N.; Ferrera, M.; Naik, G. v.; Babicheva, V. E.; Shalaev, V. M.; Boltasseva, A. Experimental Demonstration of Titanium Nitride Plasmonic Interconnects. *Optics Express* **2014**, *22* (10), 12238. <https://doi.org/10.1364/OE.22.012238>.
- (106) Kinsey, N.; Syed, A. A.; Courtwright, D.; DeVault, C.; Bonner, C. E.; Gavrilenko, V. I.; Shalaev, V. M.; Hagan, D. J.; van Stryland, E. W.; Boltasseva, A. Effective Third-Order Nonlinearities in Metallic Refractory Titanium Nitride Thin Films. *Optical Materials Express* **2015**, *5* (11), 2587. <https://doi.org/10.1364/ome.5.002395>.
- (107) Yang, Y.; Kelley, K.; Sachet, E.; Campione, S.; Luk, T. S.; Maria, J.-P.; Sinclair, M. B.; Brener, I. Femtosecond Optical Polarization Switching Using a Cadmium Oxide-Based Perfect Absorber. *Nature Photonics* **2017**, *11* (6), 390–395. <https://doi.org/10.1038/nphoton.2017.64>.
- (108) Lee, H. W.; Papadakis, G.; Burgos, S. P.; Chander, K.; Kriesch, A.; Pala, R.; Peschel, U.; Atwater, H. A. Nanoscale Conducting Oxide PlasMOStor. *Nano Letters* **2014**, *14* (11), 6463–6468. <https://doi.org/10.1021/nl502998z>.
- (109) Wood, M. G.; Campione, S.; Parameswaran, S.; Luk, T. S.; Wendt, J. R.; Serkland, D. K.; Keeler, G. A. Gigahertz Speed Operation of Epsilon-near-Zero Silicon Photonic Modulators. *Optica* **2018**, *5* (3), 233. <https://doi.org/10.1364/OPTICA.5.000233>.
- (110) Shirmanesh, G. K.; Sokhoyan, R.; Wu, P. C.; Atwater, H. A.; Wu, P. C.; Atwater, H. A.; Atwater, H. A. Electro-Optically Tunable Multifunctional Metasurfaces. *ACS Nano* **2020**, *14* (6), 6912–6920. <https://doi.org/10.1021/acsnano.0c01269>.
- (111) Huang, Y.-W. W.; Lee, H. W. H.; Sokhoyan, R.; Pala, R. A.; Thyagarajan, K.; Han, S.; Tsai, D. P.; Atwater, H. A. Gate-Tunable Conducting Oxide Metasurfaces. *Nano Letters* **2016**, *16* (9), 5319–5325. <https://doi.org/10.1021/acs.nanolett.6b00555>.
- (112) Alam, M. Z.; de Leon, I.; Boyd, R. W. Large Optical Nonlinearity of Indium Tin Oxide in Its Epsilon-near-Zero Region. *Science* **2016**, *352* (6287), 795–797. <https://doi.org/10.1126/science.aae0330>.
- (113) Reshef, O.; de Leon, I.; Alam, M. Z.; Boyd, R. W. Nonlinear Optical Effects in Epsilon-near-Zero Media. *Nature Reviews Materials* **2019**, *4* (8), 535–551. <https://doi.org/10.1038/s41578-019-0120-5>.

- (114) Galiffi, E.; Dranczewski, J.; Pendry, J.; Sapienza, R.; Tirole, R.; Maier, S.; Vezzoli, S.; Attavar, T.; Sapienza, R. Time Diffraction in an Epsilon-Near-Zero Metasurface. *Conference on Lasers and Electro-Optics (2021)*, paper FM1M.6 **2021**, FM1M.6. https://doi.org/10.1364/CLEO_QELS.2021.FM1M.6.
- (115) Bohn, J.; Luk, T. S.; Tollerton, C.; Hutchings, S. W.; Brener, I.; Horsley, S.; Barnes, W. L.; Hendry, E. All-Optical Switching of an Epsilon-near-Zero Plasmon Resonance in Indium Tin Oxide. *Nature Communications* **2021**, *12* (1), 1–6. <https://doi.org/10.1038/s41467-021-21332-y>.
- (116) Yang, Y.; Kelley, K.; Sachet, E.; Campione, S.; Luk, T. S.; Maria, J.-P.; Sinclair, M. B.; Brener, I. Femtosecond Optical Polarization Switching Using a Cadmium Oxide-Based Perfect Absorber. *Nature Photonics* **2017**, *11* (6), 390–395. <https://doi.org/10.1038/nphoton.2017.64>.
- (117) Bruno, V.; Vezzoli, S.; Devault, C.; Roger, T.; Ferrera, M.; Boltasseva, A.; Shalaev, V. M.; Faccio, D. Dynamical Control of Broadband Coherent Absorption in ENZ Films. *Micromachines (Basel)* **2020**. <https://doi.org/10.3390/mi11010110>.
- (118) Anopchenko, A.; Tao, L.; Arndt, C.; Lee, H. W. H. Field-Effect Tunable and Broadband Epsilon-Near-Zero Perfect Absorbers with Deep Subwavelength Thickness. *ACS Photonics* **2018**, *5* (7). <https://doi.org/10.1021/acsp Photonics.7b01373>.
- (119) Runnerstrom, E. L.; Kelley, K. P.; Sachet, E.; Shelton, C. T.; Maria, J.-P. Epsilon-near-Zero Modes and Surface Plasmon Resonance in Fluorine-Doped Cadmium Oxide Thin Films. **2017**. <https://doi.org/10.1021/acsp Photonics.7b00429>.
- (120) Passler, N. C.; Razdolski, I.; Katzer, D. S.; Storm, D. F.; Caldwell, J. D.; Wolf, M.; Paarmann, A. Second Harmonic Generation from Phononic Epsilon-Near-Zero Berreman Modes in Ultrathin Polar Crystal Films. *ACS Photonics* **2019**, *6* (6), 1365–1371. <https://doi.org/10.1021/ACSPHOTONICS.9B00290>.
- (121) Yang, Y.; Lu, J.; Manjavacas, A.; Luk, T. S.; Liu, H.; Kelley, K.; Maria, J.-P.; Runnerstrom, E. L.; Sinclair, M. B.; Ghimire, S.; Brener, I. High-Harmonic Generation from an Epsilon-near-Zero Material. *Nature Physics* **2019**, *15* (10), 1022–1026. <https://doi.org/10.1038/s41567-019-0584-7>.

- (122) Naik, G. v; Kim, J.; Boltasseva, A. Oxides and Nitrides as Alternative Plasmonic Materials in the Optical Range [Invited]. *Optical Materials Express* **2011**, *1* (6), 1090. <https://doi.org/10.1364/OME.1.001090>.
- (123) Zgrabik, C. M.; Hu, E. L. Optimization of Sputtered Titanium Nitride as a Tunable Metal for Plasmonic Applications. *Optical Materials Express* **2015**, *5* (12), 2786. <https://doi.org/10.1364/OME.5.002786>.
- (124) Gui, Y.; Miscuglio, M.; Ma, Z.; Tahersima, M. H.; Sun, S.; Amin, R.; Dalir, H.; Sorger, V. J. Towards Integrated Metatronics: A Holistic Approach on Precise Optical and Electrical Properties of Indium Tin Oxide. *Scientific Reports* *2019 9:1* **2019**, *9* (1), 1–10. <https://doi.org/10.1038/s41598-019-47631-5>.
- (125) Saha, S.; Diroll, B. T.; Shank, J.; Kudyshev, Z.; Dutta, A.; Chowdhury, S. N.; Luk, T. S.; Campione, S.; Schaller, R. D.; Shalaev, V. M.; Boltasseva, A.; Wood, M. G. Broadband, High-Speed, and Large-Amplitude Dynamic Optical Switching with Yttrium-Doped Cadmium Oxide. *Advanced Functional Materials* **2020**, *30* (7), 1908377. <https://doi.org/10.1002/adfm.201908377>.
- (126) Liu, H.-D.; Zhao, Y.-P.; Ramanath, G.; Murarka, S. P.; Wang, G.-C. Thickness Dependent Electrical Resistivity of Ultrathin (<40 Nm) Cu Films. *Thin Solid Films* **2001**, *384* (1), 151–156. [https://doi.org/10.1016/S0040-6090\(00\)01818-6](https://doi.org/10.1016/S0040-6090(00)01818-6).
- (127) Dong, B. Z.; Fang, G. J.; Wang, J. F.; Guan, W. J.; Zhao, X. Z. Effect of Thickness on Structural, Electrical, and Optical Properties of ZnO: Al Films Deposited by Pulsed Laser Deposition. *Journal of Applied Physics* **2007**, *101* (3). <https://doi.org/10.1063/1.2437572>.
- (128) Gilani, T. H.; Rabchuk, D. Electrical Resistivity of Gold Thin Film as a Function of Film Thickness. *Canadian Journal of Physics* **2018**, *96* (3), 272–274. <https://doi.org/10.1139/CJP-2017-0484/ASSET/IMAGES/CJP-2017-0484IEQ8.GIF>.
- (129) Kim, H.; Horwitz, J. S.; Kushto, G. Cite As. *Journal of Applied Physics* **2000**, *88*, 6021. <https://doi.org/10.1063/1.1318368>.
- (130) Tanaka, K.; Fujita, K.; Kamakura, R.; Yasuhara, R.; Murai, S.; Daido, Y. Plasmonic Arrays of Titanium Nitride Nanoparticles Fabricated from Epitaxial Thin Films. *Optics Express*, *Vol. 24, Issue 2, pp. 1143-1153* **2016**, *24* (2), 1143–1153. <https://doi.org/10.1364/OE.24.001143>.

- (131) Shah, D.; Reddy, H.; Kinsey, N.; Shalaev, V. M.; Boltasseva, A. Optical Properties of Plasmonic Ultrathin TiN Films. *Advanced Optical Materials* **2017**, *5* (13), 1700065. <https://doi.org/10.1002/ADOM.201700065>.
- (132) Izyumskaya, N.; Fomra, D.; Ding, K.; Morkoç, H.; Kinsey, N.; Özgür, Ü.; Avrutin, V. High-Quality Plasmonic Materials TiN and ZnO:Al by Atomic Layer Deposition. *physica status solidi (RRL) – Rapid Research Letters* **2021**, *15* (10), 2100227. <https://doi.org/10.1002/PSSR.202100227>.
- (133) Gadalla, M. N.; Greenspon, A. S.; Tamagnone, M.; Capasso, F.; Hu, E. L. Excitation of Strong Localized Surface Plasmon Resonances in Highly Metallic Titanium Nitride Nano-Antennas for Stable Performance at Elevated Temperatures. *ACS Applied Nano Materials* **2019**, *2* (6), 3444–3452. <https://doi.org/10.1021/ACSANM.9B00370>.
- (134) Reese, T.; Reed, A. N.; Sample, A. D.; Freire-Fernández, F.; Schaller, R. D.; Urbas, A. M.; Odom, T. W. Ultrafast Spectroscopy of Plasmonic Titanium Nitride Nanoparticle Lattices. *ACS Photonics* **2021**, *8* (6), 1556–1561. <https://doi.org/10.1021/acsp Photonics.1c00297>.
- (135) Sugavaneshwar, R. P.; Ishii, S.; Dao, T. D.; Ohi, A.; Nabatame, T.; Nagao, T. Fabrication of Highly Metallic TiN Films by Pulsed Laser Deposition Method for Plasmonic Applications. *ACS Photonics* **2017**, *5* (3), 814–819. <https://doi.org/10.1021/ACSPHOTONICS.7B00942>.
- (136) Sun, R.; Makise, K.; Qiu, W.; Terai, H.; Wang, Z. Fabrication of (200)-Oriented TiN Films on Si (100) Substrates by DC Magnetron Sputtering. *IEEE Transactions on Applied Superconductivity* **2015**, *25* (3). <https://doi.org/10.1109/TASC.2014.2383694>.
- (137) Wooten, F. OPTICAL PROPERTIES OF SOLIDS. **1972**.
- (138) Izyumskaya, N.; Fomra, D.; Ding, K.; Morkoç, H.; Kinsey, N.; Özgür, Ü.; Avrutin, V. High-Quality Plasmonic Materials TiN and ZnO:Al by Atomic Layer Deposition. *physica status solidi (RRL) – Rapid Research Letters* **2021**, *15* (10), 2100227. <https://doi.org/10.1002/PSSR.202100227>.
- (139) Berini, P. Figures of Merit for Surface Plasmon Waveguides. *Optics Express* **2006**, *14* (26), 13030. <https://doi.org/10.1364/OE.14.013030>.
- (140) Christine M. Zgrabik; Evelyn L. Hu. Optimization of Sputtered Titanium Nitride as a Tunable Metal for Plasmonic Applications. *Optical Materials Express* **2015**, *51* (12). <https://doi.org/10.1364/OME.5.002786>.

- (141) Fomra, D.; Secondo, R.; Ding, K.; Avrutin, V.; Izyumskaya, N.; Özgür, Ü.; Kinsey, N. Plasmonic Titanium Nitride via Atomic Layer Deposition: A Low-Temperature Route. *J. Appl. Phys* **2020**, *127*, 103101. <https://doi.org/10.1063/1.5130889>.
- (142) Hu, J.; Ren, X.; Reed, A. N.; Reese, T.; Rhee, D.; Howe, B.; Lauhon, L. J.; Urbas, A. M.; Odom, T. W. Evolutionary Design and Prototyping of Single Crystalline Titanium Nitride Lattice Optics. **2017**. <https://doi.org/10.1021/acsp Photonics.6b00955>.
- (143) Pasupathi Sugavaneshwar, R.; Ishii, S.; Thang, †; Dao, D.; Ohi, A.; Nabatame, T.; Nagao, T. Fabrication of Highly Metallic TiN Films by Pulsed Laser Deposition Method for Plasmonic Applications. *ACS Photonics* **2018**, *5*, 819. <https://doi.org/10.1021/acsp Photonics.7b00942>.
- (144) Capretti, A.; Wang, Y.; Engheta, N.; Dal Negro, L. Comparative Study of Second-Harmonic Generation from Epsilon-Near-Zero Indium Tin Oxide and Titanium Nitride Nanolayers Excited in the Near-Infrared Spectral Range. *ACS Photonics* **2015**, *2*, 1584–1591. <https://doi.org/10.1021/acsp Photonics.5b00355>.
- (145) Capretti, A.; Wang, Y.; Engheta, N.; Dal Negro, L. Comparative Study of Second-Harmonic Generation from Epsilon-Near-Zero Indium Tin Oxide and Titanium Nitride Nanolayers Excited in the Near-Infrared Spectral Range. *ACS Photonics* **2015**, *2* (11), 1584–1591. https://doi.org/10.1021/ACSPHOTONICS.5B00355/ASSET/IMAGES/ACSPHOTONICS.5B00355.SOCIAL.JPEG_V03.
- (146) Huber, P.; Manova, D.; Mändl, S.; Rauschenbach, B. Optical Characterization of TiN Produced by Metal-Plasma Immersion Ion Implantation. *Surface and Coatings Technology* **2001**, *142–144*, 418–423. [https://doi.org/10.1016/S0257-8972\(01\)01082-9](https://doi.org/10.1016/S0257-8972(01)01082-9).
- (147) Patsalas, P.; Logothetidis, S. Optical, Electronic, and Transport Properties of Nanocrystalline Titanium Nitride Thin Films. *Journal of Applied Physics* **2001**, *90* (9), 4725. <https://doi.org/10.1063/1.1403677>.
- (148) Ishii, S.; Sugavaneshwar, R. P.; Nagao, T. Titanium Nitride Nanoparticles as Plasmonic Solar Heat Transducers. **2015**. <https://doi.org/10.1021/acs.jpcc.5b09604>.
- (149) Langereis, E.; Heil, S. B. S.; van de Sanden, M. C. M.; Kessels, W. M. M. In Situ Spectroscopic Ellipsometry Study on the Growth of Ultrathin TiN Films by Plasma-Assisted Atomic Layer Deposition. *Journal of Applied Physics* **2006**, *100* (2), 023534. <https://doi.org/10.1063/1.2214438>.

- (150) Fomra, D.; Mamun, M.; Ding, K.; Avrutin, V.; Özgür, Ü.; Kinsey, N. Plasmonic Colors in Titanium Nitride for Robust and Covert Security Features. *Optics Express* **2021**, *29* (13). <https://doi.org/10.1364/OE.423155>.
- (151) Gall, D.; Petrov, I.; Greene, J. E. Epitaxial $\text{Sc}_{1-x}\text{Ti}_x\text{N}$: Optical and Electronic Transport Properties. **2001**. <https://doi.org/10.1063/1.1329348>.
- (152) Maurya, K. C.; Maurya, K. C.; Maurya, K. C.; Shalaev, V. M.; Boltasseva, A.; Saha, B.; Saha, B.; Saha, B.; Saha, B. Reduced Optical Losses in Refractory Plasmonic Titanium Nitride Thin Films Deposited with Molecular Beam Epitaxy. *Optical Materials Express*, *Vol. 10, Issue 10*, pp. 2679-2692 **2020**, *10* (10), 2679–2692. <https://doi.org/10.1364/OME.405259>.
- (153) Guo, W. P.; Mishra, R.; Cheng, C. W.; Wu, B. H.; Chen, L. J.; Lin, M. T.; Gwo, S. Titanium Nitride Epitaxial Films as a Plasmonic Material Platform: Alternative to Gold. *ACS Photonics* **2019**, *6* (8), 1848–1854. <https://doi.org/10.1021/acsp Photonics.9b00617>.
- (154) Jeyachandran, Y. L.; Narayandass, S. K.; Mangalaraj, D.; Areva, S.; Mielczarski, J. A. Properties of Titanium Nitride Films Prepared by Direct Current Magnetron Sputtering. *Materials Science and Engineering: A* **2007**, *445–446*, 223–236. <https://doi.org/10.1016/J.MSEA.2006.09.021>.
- (155) Ribbing, C.-G.; Valkonen, E.; Sundgren, J.-E. Optical Constants of Thin TiN Films: Thickness and Preparation. *Applied Optics*, *Vol. 25, Issue 20*, pp. 3624-3630 **1986**, *25* (20), 3624–3630. <https://doi.org/10.1364/AO.25.003624>.
- (156) Martin, P.; Netterfield, R.; Sainty, W. Optical Properties of TiN_x Produced by Reactive Evaporation and Reactive Ion-Beam Sputtering. *Vacuum* **1982**, *32* (6), 359–362. [https://doi.org/10.1016/0042-207X\(82\)93829-5](https://doi.org/10.1016/0042-207X(82)93829-5).
- (157) Shah, D.; Reddy, H.; Kinsey, N.; Shalaev, V. M.; Boltasseva, A. Optical Properties of Plasmonic Ultrathin TiN Films. *Advanced Optical Materials* **2017**, *5* (13), 1–5. <https://doi.org/10.1002/adom.201700065>.
- (158) Luka, G.; Krajewski, T. A.; Witkowski, B. S.; Wisz, G.; Virt, I. S.; Guziewicz, E.; Godlewski, M. Aluminum-Doped Zinc Oxide Films Grown by Atomic Layer Deposition for Transparent Electrode Applications. *Journal of Materials Science: Materials in Electronics* **2011**, *22* (12), 1810–1815. <https://doi.org/10.1007/S10854-011-0367-0/FIGURES/7>.

- (159) Wong, L. M.; Chiam, S. Y.; Chim, W. K.; Pan, J. S.; Wang, S. J. Highly Conductive and Transparent Aluminum-Doped Zinc Oxide Thin Films Deposited on Polyethylene Terephthalate Substrates by Pulsed Laser Deposition. *Thin Solid Films* **2013**, *545*, 285–290. <https://doi.org/10.1016/J.TSF.2013.08.069>.
- (160) Suzuki, A.; Nakamura, M.; Michihata, R.; Aoki, T.; Matsushita, T.; Okuda, M. Ultrathin Al-Doped Transparent Conducting Zinc Oxide Films Fabricated by Pulsed Laser Deposition. *Thin Solid Films* **2008**, *517* (4), 1478–1481. <https://doi.org/10.1016/J.TSF.2008.09.024>.
- (161) Dong, B.-Z.; Fang, G.-J.; Wang, J.-F. Effect of Thickness on Structural, Electrical, and Optical Properties of ZnO: Al Films Deposited by Pulsed Laser Deposition. *J. Appl. Phys* **2007**, *101*, 33713. <https://doi.org/10.1063/1.2437572>.
- (162) Liberal, I.; Engheta, N. Near-Zero Refractive Index Photonics. *Nature Photonics* **2017** *11*:3 **2017**, *11* (3), 149–158. <https://doi.org/10.1038/nphoton.2017.13>.
- (163) Clerici, M.; Kinsey, N.; DeVault, C.; Kim, J.; Carnemolla, E. G.; Caspani, L.; Shaltout, A.; Faccio, D.; Shalaev, V.; Boltasseva, A.; Ferrera, M. Controlling Hybrid Nonlinearities in Transparent Conducting Oxides via Two-Colour Excitation. *Nat Commun* **2017**, *8* (1), 15829. <https://doi.org/10.1038/ncomms15829>.
- (164) Liu, C.; Alam, M. Z.; Pang, K.; Manukyan, K.; Reshef, O.; Zhou, Y.; Choudhary, S.; Patrow, J.; Pennathurs, A.; Song, H.; Zhao, Z.; Zhang, R.; Alishahi, F.; Fallahpour, A.; Cao, Y.; Almainan, A.; Dawlaty, J. M.; Tur, M.; Boyd, R. W.; Willner, A. E. Photon Acceleration Using a Time-Varying Epsilon-near-Zero Metasurface. *ACS Photonics* **2021**. <https://doi.org/10.1021/acsp Photonics.0c01929>.
- (165) Diroll, B. T.; Saha, S.; Shalaev, V. M.; Boltasseva, A.; Schaller, R. D. Broadband Ultrafast Dynamics of Refractory Metals: TiN and ZrN. *Advanced Optical Materials* **2020**, *8* (19), 2000652. <https://doi.org/10.1002/ADOM.202000652>.
- (166) Berini, P. Long-Range Surface Plasmon Polaritons. *Advances in Optics and Photonics* **2009**, *1* (3), 484. <https://doi.org/10.1364/aop.1.000484>.
- (167) Vassant, S.; Hugonin, J.-P.; Marquier, F.; Greffet, J.-J. Berreman Mode and Epsilon near Zero Mode. *Optics Express* **2012**, *20* (21), 23971. <https://doi.org/10.1364/oe.20.023971>.

- (168) Campione, S.; Brener, I.; Marquier, F. Theory of Epsilon-near-Zero Modes in Ultrathin Films. *RAPID COMMUNICATIONS PHYSICAL REVIEW B* **2015**, *91*, 121408. <https://doi.org/10.1103/PhysRevB.91.121408>.
- (169) Ferrell, R. A. Predicted Radiation of Plasma Oscillations in Metal Films. *Physical Review* **1958**, *111* (5), 1214. <https://doi.org/10.1103/PhysRev.111.1214>.
- (170) Berreman, D. W. Infrared Absorption at Longitudinal Optic Frequency in Cubic Crystal Films. *Physical Review* **1963**, *130* (6), 2193. <https://doi.org/10.1103/PhysRev.130.2193>.
- (171) Yang, Z.; Ji, C.; Liu, D.; Guo, L. J.; Yang, Z.; Ji, C.; Guo, L. J.; Liu, D. Enhancing the Purity of Reflective Structural Colors with Ultrathin Bilayer Media as Effective Ideal Absorbers. *Advanced Optical Materials* **2019**, *7* (21), 1900739. <https://doi.org/10.1002/ADOM.201900739>.
- (172) Kats, M. A.; Capasso, F. *Optical Absorbers Based on Strong Interference in Ultra-Thin Films*; 2016. <https://doi.org/10.1002/lpor.201600098>.
- (173) Kats, M. A.; Blanchard, R.; Genevet, P.; Capasso, F. Nanometre Optical Coatings Based on Strong Interference Effects in Highly Absorbing Media. *Nature Materials* **2013**, *12* (1), 20–24. <https://doi.org/10.1038/NMAT3443>.
- (174) Anopchenko, A.; Tao, L.; Arndt, C.; Lee, H. W. H. Field-Effect Tunable and Broadband Epsilon-Near-Zero Perfect Absorbers with Deep Subwavelength Thickness. *ACS Photonics* **2018**, *5* (7), 2631–2637. <https://doi.org/10.1021/acsp Photonics.7b01373>.
- (175) Saleh, B. E. A.; Teich, M. C. *Fundamentals of Photonics*. **1991**. <https://doi.org/10.1002/0471213748>.
- (176) Anopchenko, A.; Gurung, S.; Bej, S.; Wai, H.; Lee, H. Field Enhancement of Epsilon-near-Zero Modes in Realistic Ultra-Thin Absorbing Films. *Physical Review Letters* **2020**.
- (177) Gurung, S.; Anopchenko, A.; Bej, S.; Joyner, J.; Myers, J. D.; Frantz, J.; Lee, H. W. H. Atomic Layer Engineering of Epsilon-Near-Zero Ultrathin Films with Controllable Field Enhancement. *Advanced Materials Interfaces* **2020**, *7* (17), 2000844. <https://doi.org/10.1002/admi.202000844>.
- (178) Zhou, Y.; Alam, M. Z.; Karimi, M.; Upham, J.; Reshef, O.; Liu, C.; Willner, A. E.; Boyd, R. W. Broadband Frequency Translation through Time Refraction in an Epsilon-near-Zero Material. *Nature Communications* **2020**, *11* (1), 1–7. <https://doi.org/10.1038/s41467-020-15682-2>.

- (179) Bruno, V.; Vezzoli, S.; DeVault, C.; Roger, T.; Shalaev, V. M.; Boltasseva, A.; Ferrera, M.; Clerici, M.; Dubietis, A.; Faccio, D.; Bruno, V.; DeVault, C.; Roger, T.; Shalaev, V. M.; Boltasseva, A.; Ferrera, M.; Clerici, M.; Dubietis, A.; Faccio, D. Optical Time Reversal from Time-Dependent Epsilon-Near-Zero Media. *Physical Review Letters* **2018**, *120* (4), 043902. <https://doi.org/10.1103/PhysRevLett.120.043902>.
- (180) Yang, Y.; Lu, J.; Manjavacas, A.; Luk, T. S.; Liu, H.; Kelley, K.; Maria, J.-P. P.; Runnerstrom, E. L.; Sinclair, M. B.; Ghimire, S.; Brener, I. High-Harmonic Generation from an Epsilon-near-Zero Material. *Nature Physics* **2019**, *15* (10), 1022–1026. <https://doi.org/10.1038/s41567-019-0584-7>.
- (181) Kinsey, N.; DeVault, C.; Kim, J.; Ferrera, M.; Shalaev, V. M.; Boltasseva, A. A. Epsilon-near-Zero Al-Doped ZnO for Ultrafast Switching at Telecom Wavelengths. *Optica* **2015**, *2* (7), 616–622. <https://doi.org/10.1364/OPTICA.2.000616>.
- (182) Clerici, M.; Kinsey, N.; DeVault, C.; Kim, J.; Carnemolla, E. G.; Caspani, L.; Shaltout, A.; Faccio, D.; Shalaev, V.; Boltasseva, A.; Ferrera, M. Controlling Hybrid Nonlinearities in Transparent Conducting Oxides via Two-Colour Excitation. *Nature Communications* **2017**, *8*, 15829. <https://doi.org/10.1038/ncomms15829>.
- (183) Bruno, V.; DeVault, C.; Vezzoli, S.; Kudyshev, Z.; Huq, T.; Mignuzzi, S.; Jacassi, A.; Saha, S.; Shah, Y. D.; Maier, S. A.; Cumming, D. R. S.; Boltasseva, A.; Ferrera, M.; Clerici, M.; Faccio, D.; Sapienza, R.; Shalaev, V. M. Negative Refraction in Time-Varying, Strongly-Coupled Plasmonic Antenna-ENZ Systems. *arXiv* **2019**, *124* (4). <https://doi.org/10.1103/PhysRevLett.124.043902>.
- (184) Saha, S.; Dutta, A.; DeVault, C. T.; Diroll, B. T.; Schaller, R. D.; Kudyshev, Z. A.; Xu, X.; Kildishev, A. v.; Shalaev, V. M.; Boltasseva, A. Extraordinarily Large Permittivity Modulation in Zinc Oxide for Dynamic Nanophotonics. *Materials Today* **2021**, *43*, 27–36. <https://doi.org/10.1016/j.mattod.2020.10.023>.
- (185) Guo, P.; Schaller, R. D.; Ocola, L. E.; Diroll, B. T.; Ketterson, J. B.; Chang, R. P. H. Large Optical Nonlinearity of ITO Nanorods for Sub-Picosecond All-Optical Modulation of the Full-Visible Spectrum. *Nature Communications* *2016 7:1* **2016**, *7* (1), 1–10. <https://doi.org/10.1038/ncomms12892>.

- (186) Lustig, E.; Saha, S.; Bordo, E.; DeVault, C.; Chowdhury, S. N.; Sharabi, Y.; Boltasseva, A.; Cohen, O.; Shalaev, V. M.; Segev, M. Towards Photonic Time-Crystals: Observation of a Femtosecond Time-Boundary in the Refractive Index. In *Conference on Lasers and Electro-Optics*; OSA: Washington, D.C., 2021; p FF2H.1. https://doi.org/10.1364/CLEO_QELS.2021.FF2H.1
- (187) Bohn, J.; Luk, T. S.; Tollerton, C.; Hutchings, S. W.; Brener, I.; Horsley, S.; Barnes, W. L.; Hendry, E. All-Optical Switching of an Epsilon-near-Zero Plasmon Resonance in Indium Tin Oxide. *Nature Communications* **2021**, *12* (1), 1017. <https://doi.org/10.1038/s41467-021-21332-y>.

VITA

Mustafa Goksu Ozlu earned his bachelors degree in Electrical Engineering from Middle East Technical University with high honors. He worked as an undergraduate researcher in CEMMETU computational electromagnetics lab under the supervision of Prof. Ozgur Ergul where he conducted simulations using MLFMA algorithms on plasmonic nanoresonators for biosensing applications. During his undergrads he conducted an internship at EPFL under the supervision of Prof. Hatice Altug working on surface enhanced infrared spectroscopy using resonant metasurfaces for the detection of organic molecules.

His achievements during the bachelors earned him the prestigious Fulbright Scholarship for the duration of his Master's. He started graduate studies at Purdue University working with Prof. Vladimir Shalaev, Prof. Boltasseva and Prof. Kildishev. He pointed his research focus at nonlinear optics and epsilon near zero materials. His work during the Master's resulted in two journal and two conference papers. Mustafa aims to continue an academic career and carries on his studies as a PhD student at Purdue University.